Development and Testing of Prototype Commercial Gasifier Sensor

Final Scientific/Technical Report

October 2012 – April 2015

Principal Authors:

Serguei Zelepouga
Nathan Moery
Mengbai Wu
Alexei Saveliev

June 2015

Revision Number: 1
Revision Date: April 11, 2016

DE-FE0008350

Gas Technology Institute
1700 S. Mount Prospect Rd.
Des Plaines, IL 60018

Disclaimer

This report was prepared as an account of work sponsored by an agency of the United States Government. Neither the United States Government nor any agency thereof, nor any of their employees, makes any warranty, express or implied, or assumes any legal liability or responsibility for the accuracy, completeness, or usefulness of any information, apparatus, product, or process disclosed, or represents that its use would not infringe privately owned rights. Reference herein to any specific commercial product, process, or service by trade name, trademark, manufacturer, or otherwise does not necessarily constitute or imply its endorsement, recommendation, or favoring by the United States Government or any agency thereof. The views and opinions of authors expressed herein do not necessarily state or reflect those of the United States Government or any agency thereof.

Acronyms

B	Blue
CFD	Computational Fluid Dynamics
GTI	Gas Technology Institute
IR	Infrared
NCSU	North Carolina State University
R	Red
UV	Ultraviolet
WCFOP	Water Cooled Fiber-Optic Probe

Abstract

This report is submitted to the National Energy Technology Laboratory in partial fulfillment of the contractual requirements for the project titled "Development and Testing of Prototype Commercial Gasifier Sensor" sponsored by the U.S. Department of Energy, DOE Award Number - DEFE0008350. This project is continuation of the “Real Time Flame Monitoring of Gasifier Burner and Injectors” effort conducted under DOE Co-operative Agreement Number DE-FS26-02NT41585.

This report presents the results of the sensor development and testing at the Wabash River gasifier. The project work was initiated with modification of the sensor software (Task 2) to enable real time temperature data acquisition, and to process and provide the obtained gasifier temperature information to the gasifier operators. The software modifications were conducted by the North Carolina State University (NCSU) researchers. The modified software was tested at the Gas Technology Institute (GTI) combustion laboratory to assess the temperature recognition algorithm accuracy and repeatability. Task 3 was focused on the sensor hardware modifications needed to improve reliability of the sensor system. NCSU conducted numerical modeling of the sensor probe’s purging flow. Based on the modeling results the probe purging system was redesigned to prevent carbon particulates deposition on the probe’s sapphire window. The modified design was evaluated and approved by the Wabash representative. The modified gasifier sensor was built and installed at the Wabash River gasifier on May 1 2014. (Task 4) The sensor was tested from the startup of the gasifier on May 5, 2015 until the planned autumn gasifier outage starting in the beginning of October, 2015. (Task 5) The project team successfully demonstrated the Gasifier Sensor system’s ability to monitor gasifier temperature while maintaining unobstructed optical access for six months without any maintenance. The sensor examination upon completion of the trial revealed that the system did not sustain any damage.

Table of Contents

Disclaimer 1
Acronyms 2
Abstract 3
Introduction 7
Project Objectives 8
Scope of Work 8
Accomplishments 12
  Task 2.0 Sensor Software and Data Acquisition Development 12
    Development of Gasifier Sensor software 12
    Laboratory testing of the Gasifier Sensor with the new software 14
  Task 3.0 Design of the Purging System 21
    Numerical Modeling of the purging flow 21
    Laboratory Testing of the Purging System 28
    Design Modifications 45
  Task 4.0 Sensor Modification and Installation at the Wabash River Gasifier 48
  Task 5.0 Sensor Testing at the Wabash River Gasifier 51
    Maintaining unobstructed optical access 51
    Performance of the Gasifier Sensor software during the first two months of testing 53
    Temperature monitoring results 53
  Task 7.0 Development of Commercialization Plan 55

List of Tables

Table 1. Measured flow rate, calculated flow rate, calculated maximum average velocity, and local Reynolds number. The kinematic viscosity of air was taken to be 1.57 10^{-2} cm^2/s. 34

List of Figures

Figure 1. Software modes 13
Figure 2. Engineer mode control screen 14
Figure 3. Operator mode control screen 14
Figure 4. Diagram of the gasifier sensor testing setup 15
Figure 5. Photograph of the Gasifier Sensor testing setup 15
Figure 6. Calibration 1, linear fit 16
Figure 7. Calibration 2, polynomial fit 16
Figure 8. Comparison of temperature measurements obtained with Gasifier Sensor using Calibration 1 and the contact temperature sensor of the Black body 17
Figure 9. Comparison of temperature measurements obtained with Gasifier Sensor using Calibration 2 and the contact temperature sensor of the Black body 18
Figure 10. High temperature furnace setup 19
Figure 11. Measurement of the furnace refractory temperature using linear approximation 20
Figure 12. Measurement of the furnace refractory temperature using polynomial approximation... 20
Figure 13. Dimensioned (a) and trimetric (b) drawings of optical system and channel. 22
Figure 14. Original geometry and mesh 23
Figure 15. Simulation boundary conditions 23
Figure 16. Streamlines on the symmetric surface (original geometry) 24
Figure 17. Model with separation area flatten to diffuse fluid flow 25
Figure 18. Model with obstacle on the inner wall of the flow channel 26
Figure 19. Models with taller obstacles on the inner wall of the flow channel 27
Figure 20. Optimized model based on Approach 2 28
Figure 21. Diagram of the experimental setup for purging studies 30
Figure 22. Photo of the experimental setup 31

Figure 23. Photographic results of turbulent combustion chamber experiment. Flow rates of (a) 0.0 SCFM, (b) 0.8 SCFM, (c) 1.2 SCFM, and (d) 2.0 SCFM. Highlighted box shows area free of combustion chamber contamination. 35
Figure 24. Photographic results of stagnant combustion chamber experiment. Flow rates of (a) 0.2 SCFM, (b) 0.4 SCFM, (c) 0.6 SCFM, and (d) 0.8 SCFM. Boxes highlight combustion chamber gas penetration into optical channel. 36
Figure 25. Dimensioned drawing of experimental Obstruction 1 43
Figure 26. Dimensioned drawing of experimental Obstruction 2 43
Figure 27. Experimental images of the flow in the optical channel modified using the obstruction with Configuration 1: (a) 0.1 SCFM, (b) 0.2 SCFM, (c) 0.4 SCFM, (d) 0.5 SCFM, (e) 0.7 SCFM. 44
Figure 28. Original design of the optical window assembly 45
Figure 29. Numerical simulation of the nitrogen purging flow around the original window assembly 46
Figure 30. Visualization of the purging flow around the original window assembly 46
Figure 31. Modified design of the nitrogen purging channel 47
Figure 32. Numerical simulation of the nitrogen purging flow around the modified window assembly 47
Figure 33. Visualization of the purging flow around the modified window assembly 47
Figure 34. Schematic of Sensor Installation at Wabash River Gasifier 48
Figure 35. General schematic of the water cooled fiber-optic probe 49
Figure 36. Probe assembly 50
Figure 37. Installation location 51
Figure 38. Sapphire window condition (Original design) after 5 weeks of testing under the previous project 52
Figure 39. Sapphire window condition (Redesigned window assembly) after 14 weeks of testing conducted under the current project 52
Figure 40. Comparison of temperature reading obtained with the gasifier 53
Figure 41. Comparison of Gasifier sensor readings with Wabash temperature estimates 54

Introduction

Technologists have long understood the rich potential of optical flame sensors to maintain burners or coal gasifier injectors at optimum performance, to decrease emissions of carbon monoxide and nitrogen oxides, to determine burner or injector wear, and to precisely turn down and adjust firing rates. Sensors monitoring broad infrared (IR), visible, and ultraviolet (UV) radiation are routinely used today to monitor flames. UV and IR sensors are built into flame safety and control devices. Conventional analog and digital cameras are used to monitor flame shape and length. These sensors allow furnace operators to manually adjust appropriate burner or coal injector controls to change flame length or firing rate as well as to maintain safe and stable combustion. The sensitivity and design of these sensors make them incapable of deeper qualitative and quantitative monitoring and analysis of complex combustion processes such as coal gasification.

UV and IR emission spectroscopy have been recognized as valuable tools for non-intrusive flame temperature, structure, and species analysis. To date, significant progress has been made in understanding the spectroscopic features of gaseous hydrocarbon flames and methane flames in particular. Less attention has been paid to spectroscopic studies of coal combustion and gasification.

The optical flame sensor currently developed at GTI is expected to extend the capabilities of existing combustion sensors. This sensor not only registers the presence of UV or IR light, but also monitors flame properties and flame position relative to the injector by collecting spatially resolved spectroscopic images of the flame radiation. The high temperatures and the chemically-active environment present in flames produces a number of excited species. Emission signatures of these species can be an effective tool for real-time active control systems and diagnostic sensors.

Project Objectives

The project objective was to develop and demonstrate a reliable, practical, and cost effective commercial prototype of the commercial Gasifier Sensor. The additional goal was to reveal the sensor capabilities of monitoring the gasifier temperature in real time. The reliable real time data provided by the new sensor was expected to enable the Wabash River gasifier operators to improve the gasifier refractory lifespan, as well as the gasification process efficiency and safety.

Scope of Work

This project included further development and demonstration of the sensor technology developed under the "Real Time Flame Monitoring of Gasifier Burner and Injectors". Work began with modification of the sensor software to enable real time temperature data acquisition, processing and providing the obtained gasifier temperature information to the gasifier operators. The second project task focused on the sensor hardware modifications needed to improve reliability of the sensor system. The modified gasifier sensor was installed at the Wabash River commercial gasifier and tested over a six month period to evaluate the sensor accuracy and durability. Finally, the project evaluated the commercial viability of the sensor system.

TECHNICAL TASKS

Task 2.0 Sensor Software and Data Acquisition Development

In this task, the Recipient developed a software package to enable the Gasifier sensor to obtain the gasifier temperature in real time and provide the temperature to the Wabash River Gasifier operators. The activities performed under this task included:

- *Development of Gasifier Sensor software and hardware specifications*. The Project team worked together with representatives of the field test site to develop the software specifications including the required temperature sampling frequency, data manipulation such as data averaging, time and area averaging, as well as graphical display format. Also the data acquisition system including computers and communication hardware were selected.

- *Development of the software and hardware procurement.* The project team developed the GS software based on the developed specifications. The hardware necessary to interface the GS with the Wabash River operators' station was procured.
- *Testing of the new hardware and software at the GTI laboratory.* The sensor hardware system, including the fiber bundle, camera, and data acquisition computer, were brought back to GTI from Wabash River Repowering facility so the entire system could be tested and calibrated using the high temperature electric furnace available at GTI.

Task 3.0 Design of the Purging System

In this Task the project team developed a new purging system configuration which allowed eliminating the deposition of fine black ash on the optical probe's window during sensor operation. The goal was to increase the period of continuous deposit free operation up to six months.

- *Numerical modeling of the purging flow*. A numerical model was developed and necessary numerical simulations of the purging nitrogen flow around the optical window assembly were conducted. The goal of the modeling was to establish an optimum design of the window's assembly and the purging system configuration that would prevent deposition of the ash particulates on the probe's window.
- *Laboratory setup development.* Based on the new modeling results obtained under previous task a laboratory prototype was developed. The laboratory testing of the purging setup allowed validations of the numerical model.
- *Laboratory testing of the purging system prototype*. Laboratory testing of the new window assembly and the improved nitrogen purging system was conducted.

Task 4.0 Sensor Modification and Installation at the Wabash River Gasifier

During this task, the project team modified the gasifier sensor system to implement the improvements developed under the previous tasks. The modified sensor was installed at the Wabash River gasifier.

- *Modification of the Gasifier sensor system.* The project team developed modified designs of the windows assembly and purging system to implement the improvements developed under the previous tasks.

- *Gasifier Sensor preparation and installation in Wabash River gasifier.* The new components of the Gasifier sensor were fabricated. The water cooled probe was modified to allow implementation of the new purging system. The gasifier sensor system was assembled and installed. Necessary connections were made to enable the Wabash gasifier operators to access the gasifier sensor data.
- *Preliminary testing.* Prior to the installation the sensor assembly was tested to verify that the sensor components suffered no damage during the sensor transportation to the test site. Specifically the integrity of the fiber and other optical components was verified by testing the sensor ability to collect images.

Task 5.0 Sensor Testing at the Wabash River Gasifier

The Gasifier sensor's ability to acquire the gasifier interior temperature and provide data to the gasifier operators in near real time was tested. The goal of the task was to demonstrate that the sensor is capable of continuous real time temperature monitoring over a six month period.

- *Testing the sensor interface with the Wabash River operator's working station.* The sensor interface's ability to provide real time temperature information was tested. The software was modified based on the results of the tests and comments received from the gasifier operators.
- *Testing the accuracy of the temperature measurements.* Temperature data collected over a seven day period was compared with other data/information related to the temperature of the gasifier at the same location.
- *Long term testing.* The sensor was programmed to record the temperature of the gasifier over a six month period. The condition of the optical window was continuously monitored and recorded.

Task 6.0 Analysis and Reporting

The project team prepared and submitted required quarterly reports as specified in the Federal Assistance Reporting Checklist and the Deliverables section of the Statement of Project Objectives.

Task 7.0 Development of Commercialization Plan

The proposed work was expected to complete the technology development via field verification of a Gasifier Sensor. As per the Recipient's work processes, the next logical stage in the "Stage-Gate Process for Commercialization" would be product development. Commercialization would occur when the product is readied for end-user application and is successfully brought to the marketplace. Product development and commercialization is typically undertaken by the Recipient's industrial partners since the Recipient's business model is to license its technology to industrial partners. The Recipient may, however, participate by supporting field demonstrations, deployment activities, and disseminating information about the technology/product. The Recipient will facilitate licensing opportunities by communicating the expected impact of the sensing system to industry, end-users, the technical community, and the general public. The Recipient will attempt identify suitable organizations capable of licensing and commercialization of the technology and to fully understand how its commercialization partner intends to organize their commercialization activities.

Accomplishments

Task 2.0 Sensor Software and Data Acquisition Development

In this task, the project team developed a software package to enable the Gasifier Sensor to obtain the gasifier temperature in real time and provide the temperature to the Wabash River Gasifier operators.

Development of Gasifier Sensor software

The project team developed the Gasifier Sensor software which allowed real time processing and storage of imaging data obtained by the gasifier probe.

The developed software can be operated in three modes, particularly:

- Setup mode;
- Operator mode;
- Reprocessing mode.

The functionalities for the software modes are shown in Figure 1. The setup (or engineer) mode was intended for advanced users. It contains options to define camera setup, to define calibration curves and to define area for temperature measurements. It also contains options for space and time averaging of temperatures measured by the probe.

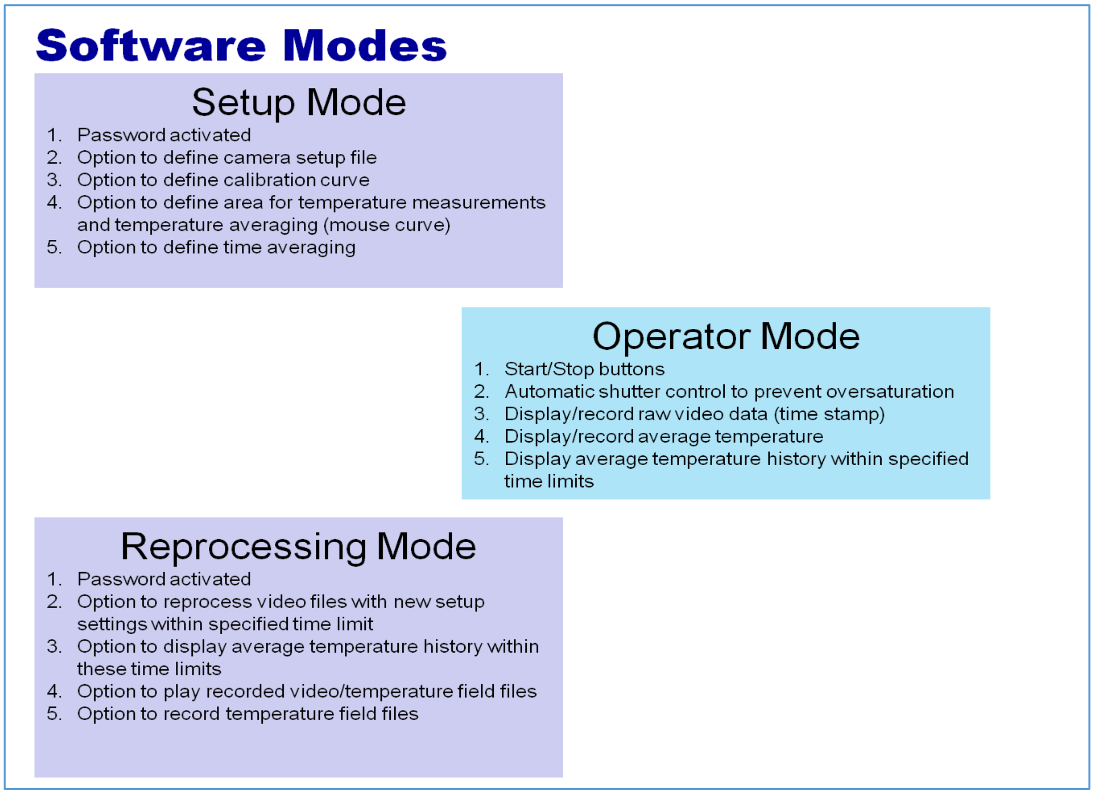

Figure 1. Software modes

The operator mode was simplified for use in the industrial environment. It contains start and stop options. It allows displaying and recording of raw video data and average temperature. The operator also can choose to display a temperature history within the specified time limits.

The configurations of the control screens for the Engineer and Operator software modes are shown in Figure 2 and Figure 3, correspondently.

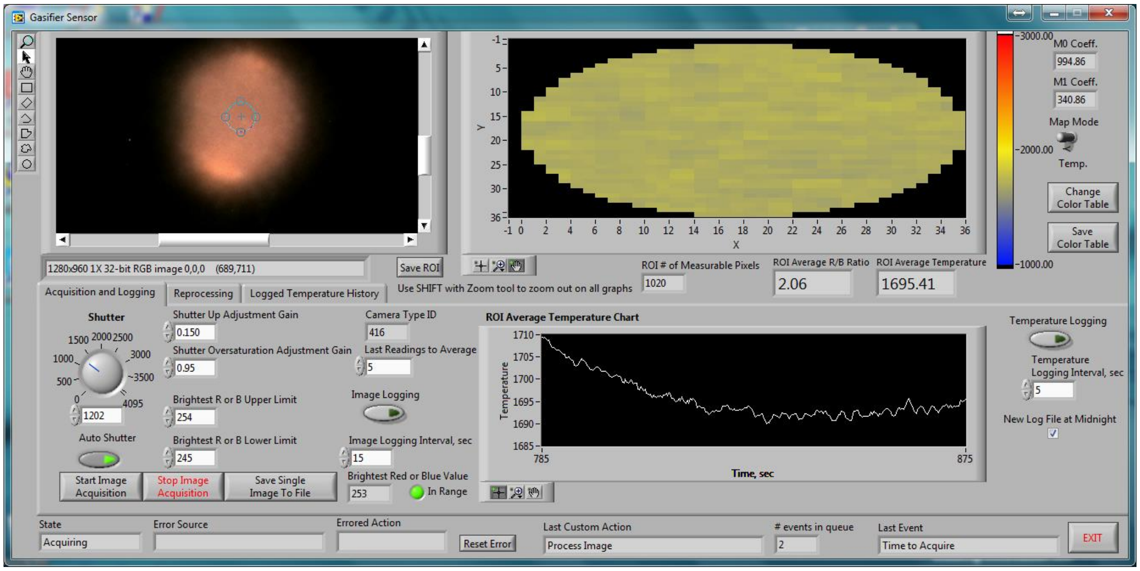

Figure 2. Engineer mode control screen

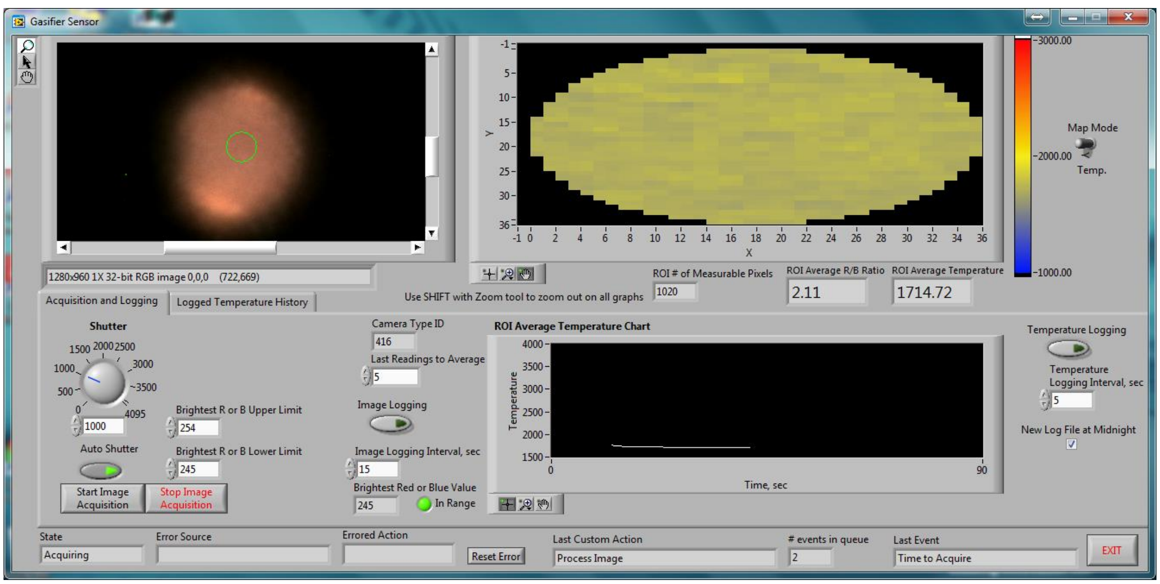

Figure 3. Operator mode control screen

Laboratory testing of the Gasifier Sensor with the new software

Prior to commencement of testing, the Gasifier Sensor was calibrated. The schematic and a photograph of the Gasifier sensor testing setup are shown in Figure 4 and Figure 5 respectively. The black body source, manufactured by Infrared Systems Development, was used to generate light emitted by Black body surfaces at temperatures from 850 °C (1562 °F) to 1200 °C (2192 °F) with 50 °C (90 °F) interval.

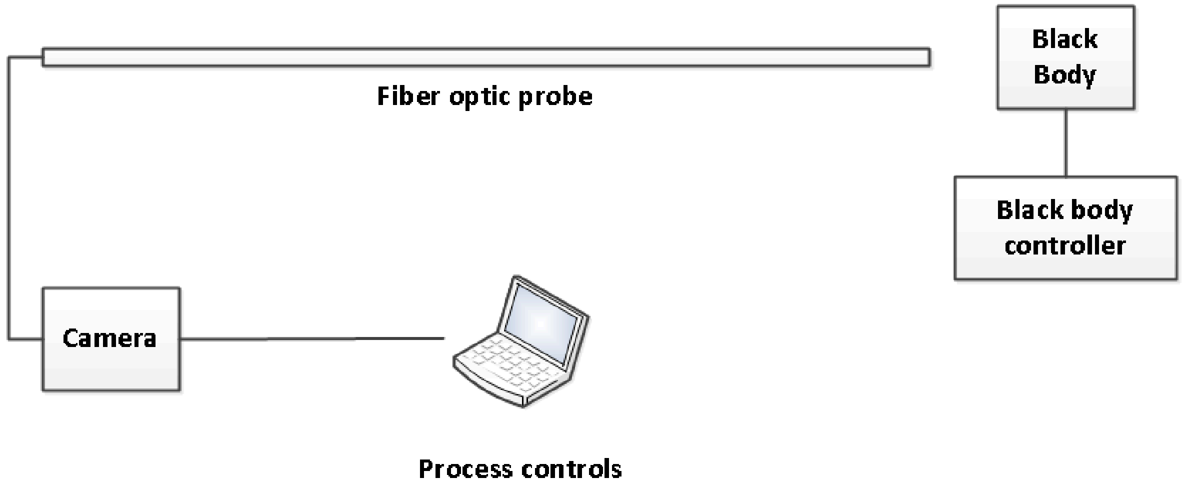

Figure 4. Diagram of the gasifier sensor testing setup

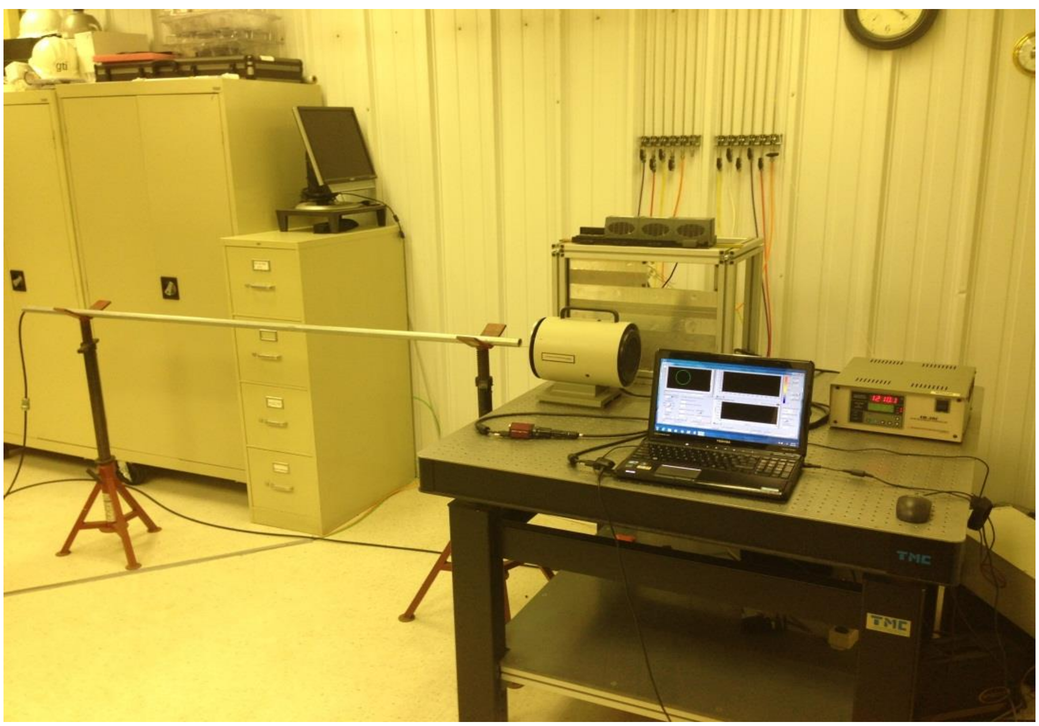

Figure 5. Photograph of the Gasifier Sensor testing setup

The new sensor software was utilized to acquire, and record images of the light emitted by the black body as well as to extract blue (B) and red (R) band intensities.

Figure 6 and Figure 7 show the temperature of Black body calibration source plotted as a function of the ratio of the R/B intensities measured with the gasifier sensor. The temperature of the radiating surface was estimated as a function of the R/B ratio as $T = M_0 + M_1$ R/B, where constants M_0 and M_1 are the linear fit coefficients. These linear fit or sensor calibration coefficients M_0=340.27 and M_1=994.86 were stored in the calibration file.

.

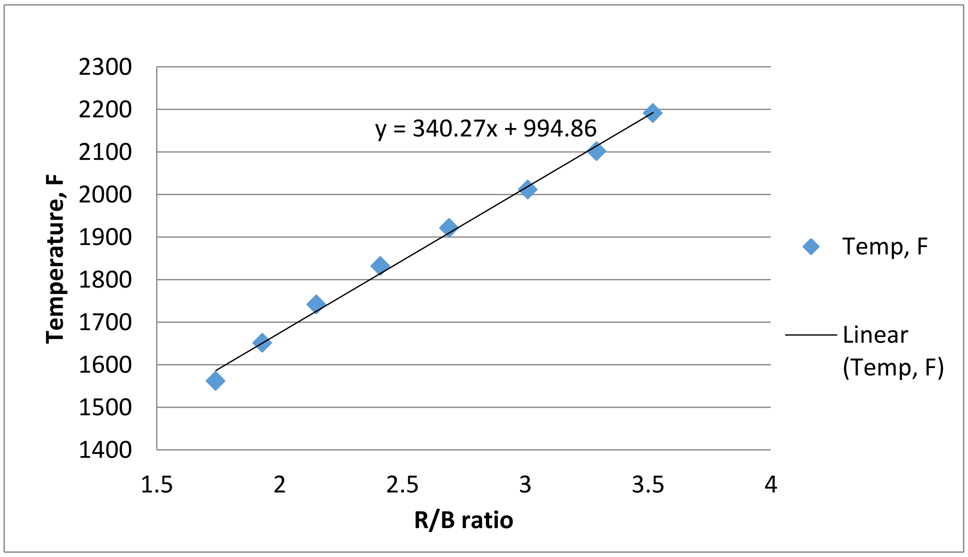

Figure 6. Calibration 1, linear fit

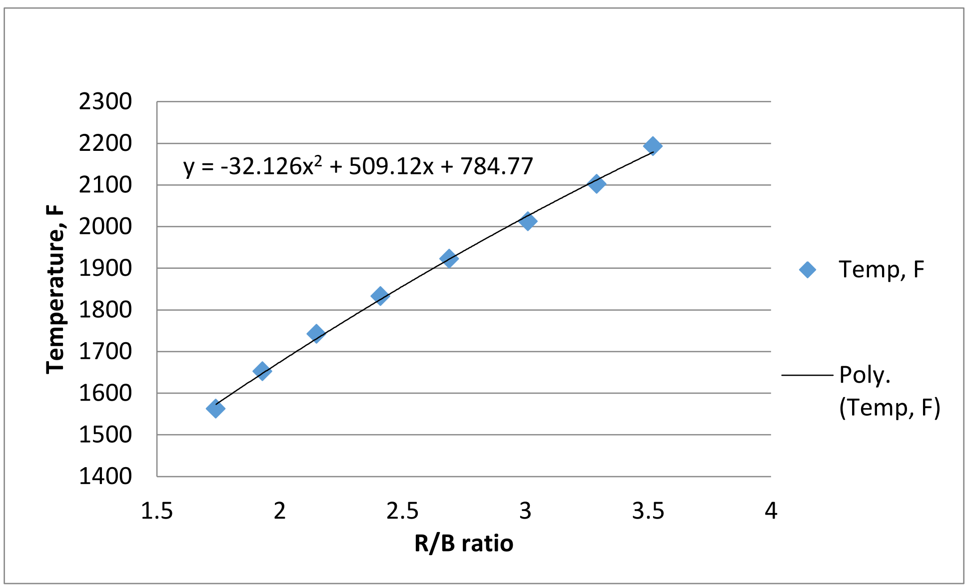

Figure 7. Calibration 2, polynomial fit

The same experimental setup already used for the sensor calibration (Figure 4 and Figure 5) was utilized to verify accuracy of the calibration algorithm. In order to assess the accuracy of the calibration the project team tested the sensor by measuring the temperature of the black body's emitting cavity and comparing the obtained temperature data with the readings of the contact temperature sensor embedded into the radiating cavity of the Black body source. The temperature of the Black body emitting cavity was varied from 850 °C (1562 °F) to 1200 °C (2192 °F) with 50 °C (90 °F) increment. Figure 8 shows comparison of the temperature measurements obtained with the Gasifier Sensor using Calibration 1 (Figure 6) and the contact temperature sensor embedded into the radiating surface of the Black body.

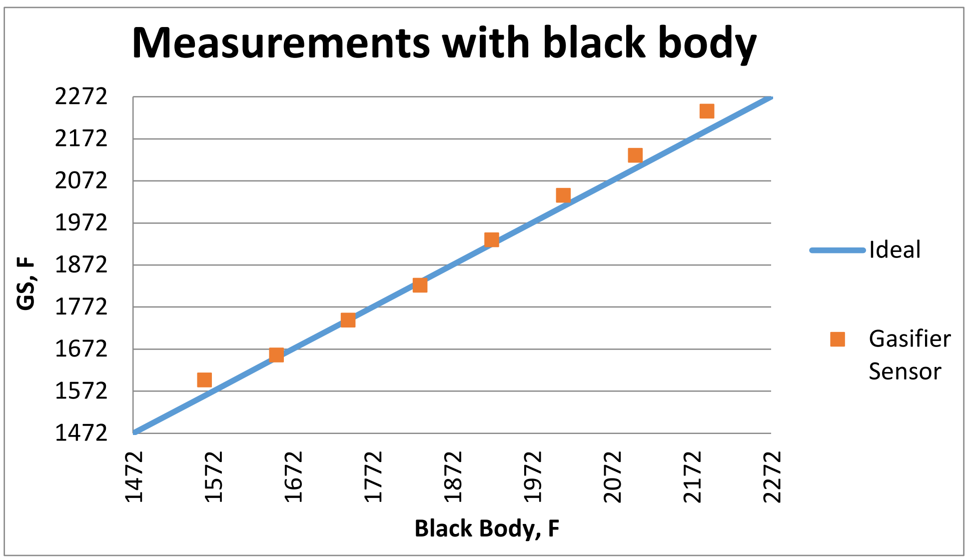

Figure 8. Comparison of temperature measurements obtained with Gasifier Sensor using Calibration 1 and the contact temperature sensor of the Black body

The blue line represents the "ideal agreement" between Gasifier Sensor data and the embedded temperature sensor. The temperature data obtained with the Gasifier Sensor agrees with the embedded sensor readings within 30 °F for most temperature points. A higher discrepancy, approximately 45 °F, was observed for the 2272 °F point. It may be an indication that the linear function selected to correlate the temperature and B/R intensities ratio may not be a good enough approximation for higher (greater than 2172 °F) temperatures.

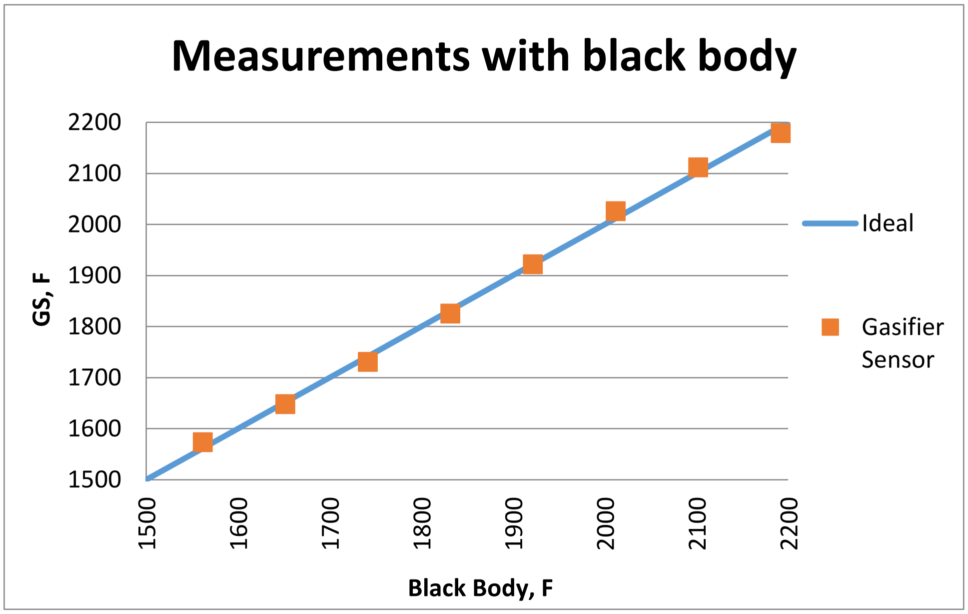

.

Figure 9. Comparison of temperature measurements obtained with Gasifier Sensor using Calibration 2 and the contact temperature sensor of the Black body

Figure 9 shows comparison of the temperature measurements obtained with the Gasifier Sensor using Calibration 2 and the temperature readings of the sensor embedded into the radiating surface of the Black body. The temperature obtained with the Gasifier sensor calibrated using polynomial correlation agrees well with the Black body sensor readings, within 20 °F

In order to confirm the results obtained during Gasifier testing using the Black body, the sensor was tested with GTI's high temperature refractory electric furnace. The photograph of the setup is shown in Figure 10.

Figure 10. High temperature furnace setup

The tests were conducted with “linear” and “polynomial” calibrations. Figure 11 and Figure 12 show the results of the tests. As observed from the graphs the polynomial calibration produced better agreement between the furnace thermocouple and Gasifier Sensor readings.

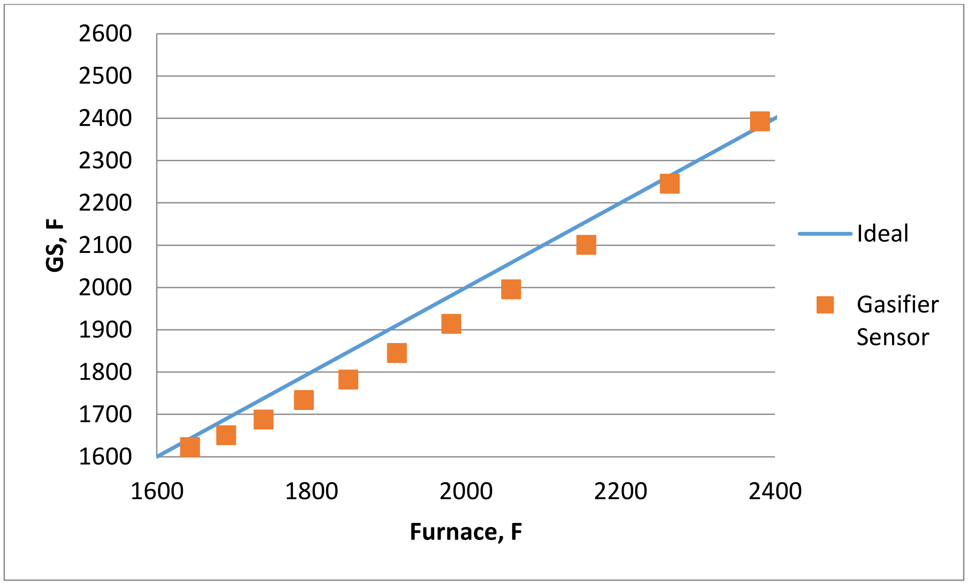

Figure 11. Measurement of the furnace refractory temperature using linear approximation

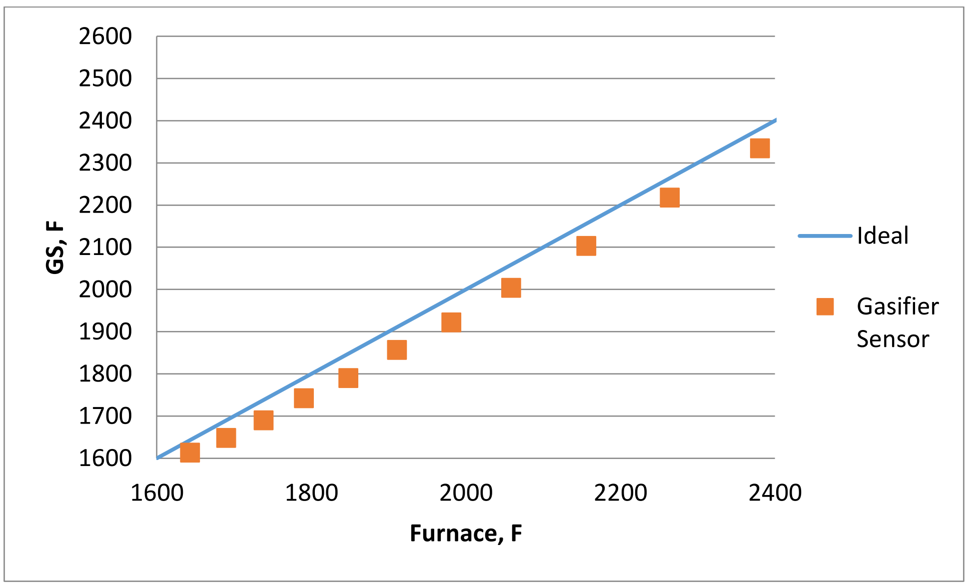

Figure 12. Measurement of the furnace refractory temperature using polynomial approximation

The Gasifier temperature readings were consistently about 50 °F lower than the thermocouple measurements. This discrepancy is likely due to the temperature non–uniformity and variation of the emission properties in the furnace enclosure.

Task 3.0 Design of the Purging System

Numerical Modeling of the purging flow

An optical system originally designed to observe the process inside the gasifier is shown in Figure 13. The optical system is composed of a lens and a holder. The system is held inside a small channel on the combustion chamber wall. The grey component in the drawing is a quarter circle representation of the lens and holder. The yellow portion is the outer wall of the channel. Dimensions are given in Figure 13(a) to give a sense of scale. Figure 13(b) is shown in a trimetric view to better visualize the system. Looking at Figure 13(a) the gasifier chamber being observed is to the right of the drawing; fluid, compressed air in experimental tests, is coming in from the left. The gasifier interior contains a large amount of coal and ash particulates.

With the current design the front surface of the viewing lens gets covered with dust quickly due to the large amount of particulate inside the chamber. In order to extend the effective operating time of the system, and to extend the required maintenance interval to an appropriate length, a reasonable revision and improvement to this system is necessary. A preliminary analysis of the local flow field, with the assumption that the dust particles generally move with the flow, suggests the drag force on the particles is dominant for particle motion.

This system is modeled with commercial package COMSOL and simulations are accordingly operated based on the actual experimental conditions. Due to the fact that the system is axially symmetric, the geometry of this system is cut through the vertical and horizontal center-lines to save calculation time. The geometry of this model is shown in Figure 14, which is the flow domain. Figure 14 also shows the mesh for the numerical calculation.

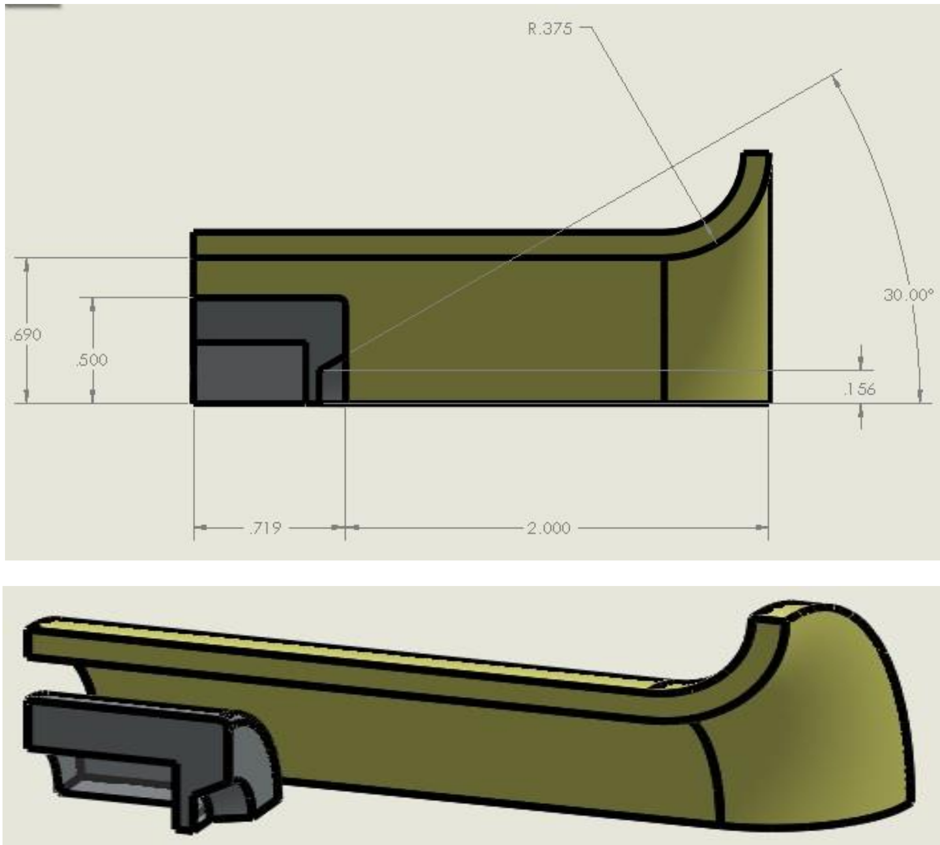

(a)

(b)

Figure 13. Dimensioned (a) and trimetric (b) drawings of optical system and channel.

The fluid used in experiments is compressed air with an entrance velocity 6 m/s. For modeling water, with an entrance velocity is 1.5 m/s, is used in addition to air at 35 atm to obtain a Reynolds number close to the actual system. The slice surfaces are set with symmetry boundary condition; all other surfaces are set up with non-slip wall condition. The boundary conditions are illustrated in Figure 15.

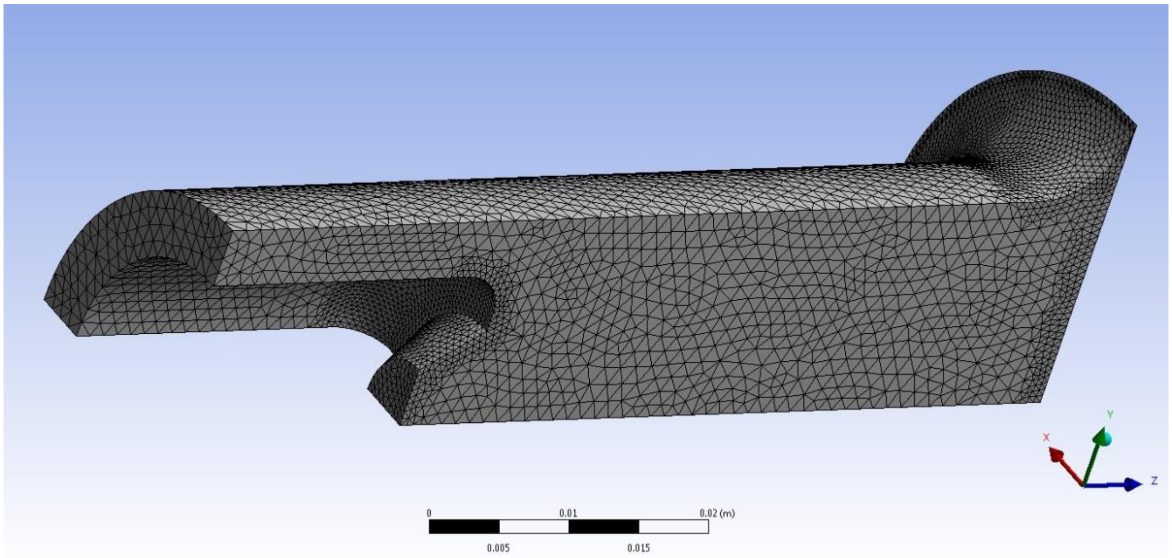

Figure 14. Original geometry and mesh

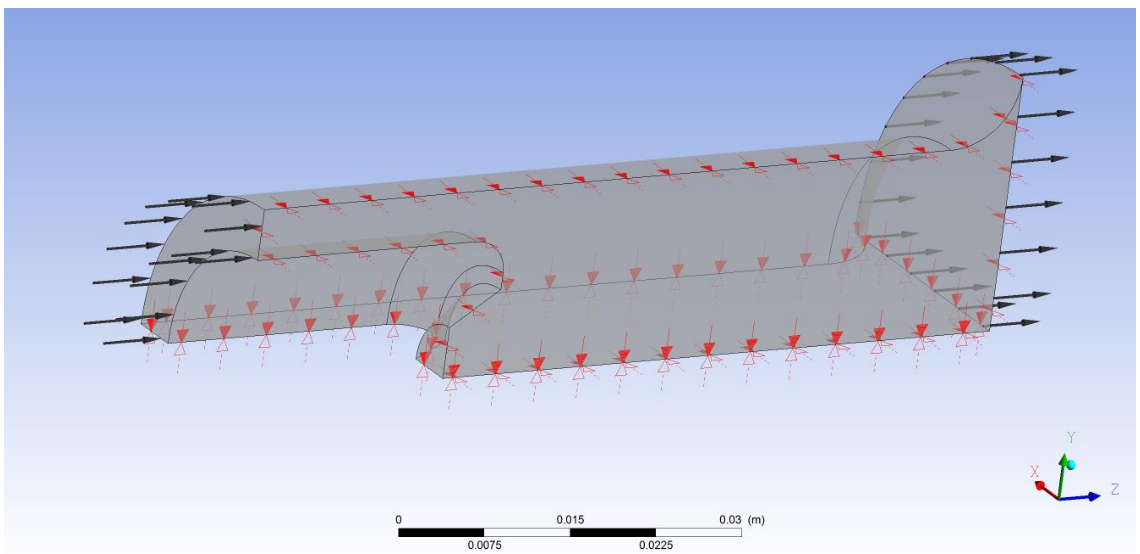

Figure 15. Simulation boundary conditions

Figure 16 shows the flow streamlines with the original equipment design. In Figure 16, an obvious circulation of fluid near the axis of the channel is shown. Recalling that the right end of the model, which is the outlet of the flow domain, is linked to the gasifier interior, this circulation is likely the reason that dust is introduced into the channel. Further observation of the streamlines in Figure 16 shows that this circulation is significant enough to deposit dust on the lens thereby blocking the view of the optical system.

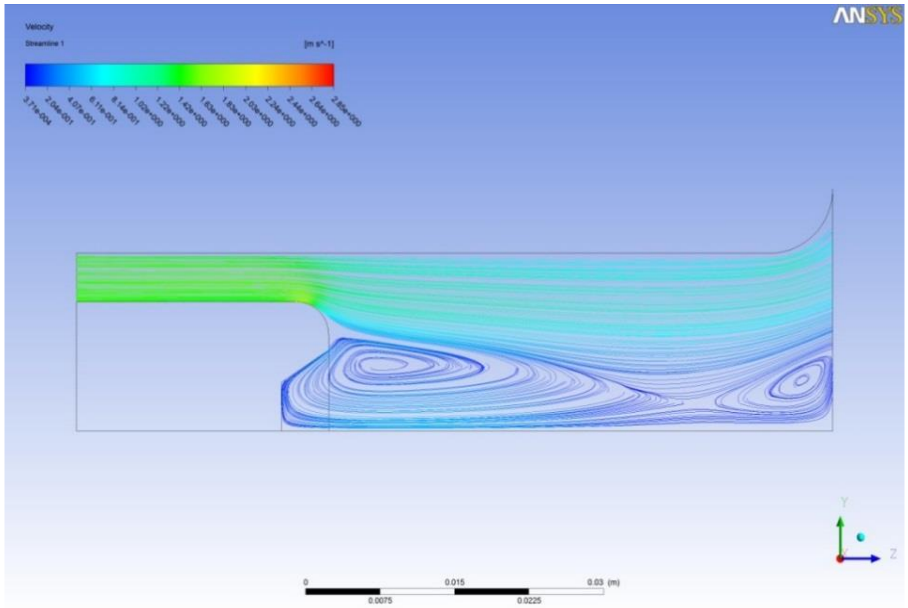

Figure 16. Streamlines on the symmetric surface (original geometry)

Two possible approaches were proposed to improve the system with the goal of breaking or eliminating the fluid recirculation observed in Figure 16. The first approach was to change the separation area of the holder; for example, flattening the corner of the holder would allow the fluid to diffuse before separation. The second approach was to change the shape of the channel. Both techniques endeavor to apply simple changes of the flow domain while achieving the primary goal of preventing fluid in the chamber from flowing into the channel. An important note is that any proposed change in the geometry of the holder or the channel must not limit the view of the lens any more than the current system.

Approach 1: Flattening the corner area of the holder.

In Figure 17, the corner area of the holder was flattened by applying a slope to the separation area. The concept here was to allow the fluid to properly diffuse before separating from the holder surface. However, comparison between Figure 16 and Figure 17 shows the slope didn’t significantly affect the circulation that was believed to be causing the particulate in the chamber to block the lens. The fact that this circulation still exists made this proposed solution ineffective.

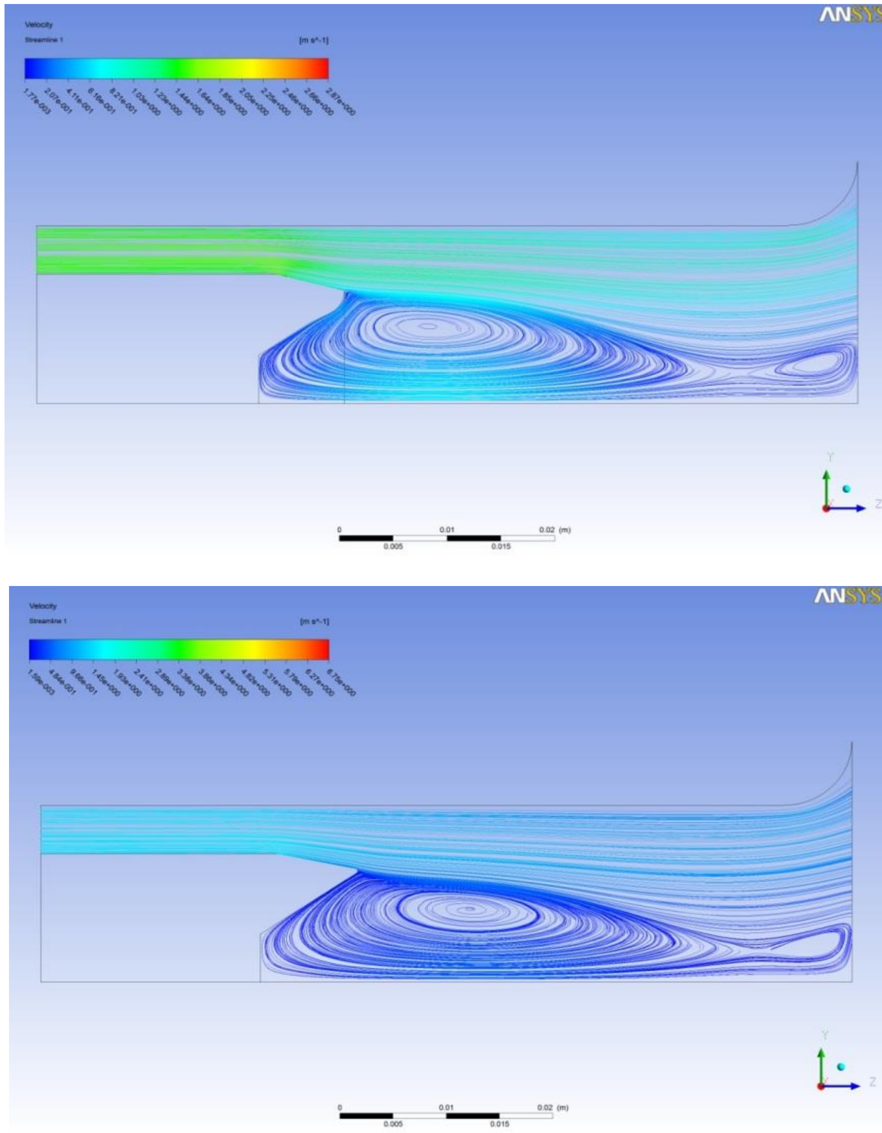

(a) (b)

Figure 17. Model with separation area flatten to diffuse fluid flow

Approach 2: Applying an obstacle on the internal surface of the channel

In this case, the flow direction was forced to flow toward the axis of the channel when the fluid passes the separation area. This forced direction of flow was created by adding a protrusion to the internal surface of the channel. This type of flow was intended to increase the possibility of clean fluid completely filling the channel thereby not allowing any combustion chamber fluid, or particulate, to enter the channel. Figure 18 shows a preliminary iteration of this solution.

However, as the figure shows, significant circulation still exists around the axis of the channel. As a matter of fact, this revision seems to make the fluid circulation worse than the original system in that the area of circulation seems to increase. Therefore this particular iteration did not seem to be a good solution to the circulation problem.

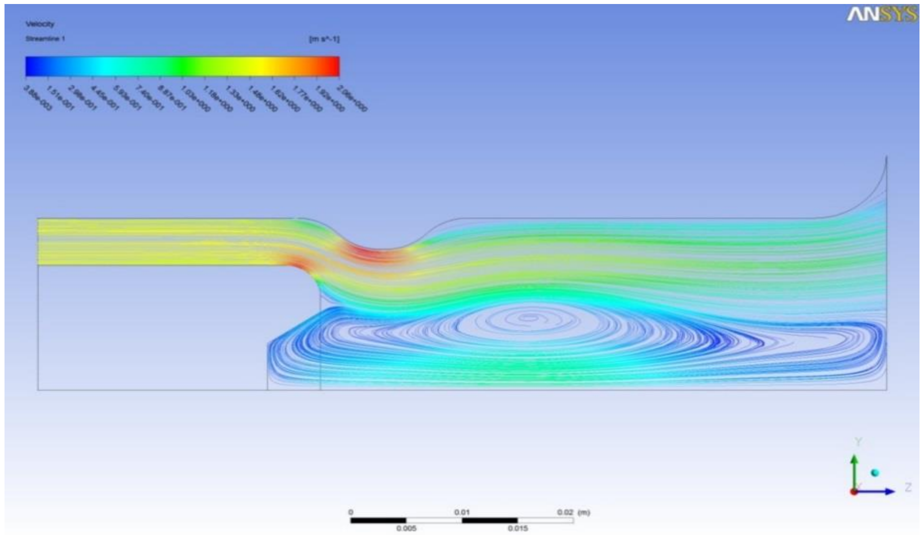

Figure 18. Model with obstacle on the inner wall of the flow channel

The above solution did, however, show the expected diversion of the flow direction. A taller obstacle may divert fluid nearer to the axis of the channel, thus reducing or eliminating circulation. However, the height of the protrusion is limited by the viewing angle of the optical system. Revised models with taller obstacles were built as in Figure 19(a-c). None of these obstacles were sufficiently large as to obstruct the view through the lens.

As shown in Figure 19, a taller obstacle diverted the flow direction even more and effectively separated the circulation. For all cases, the flow field was changed and the fluid flow from the combustion chamber into the area around the lens no longer exists. This approach is a more promising solution for the dust deposition problem than Approach 1. In the above solution, especially in the model shown in Figure 19(c), a new flow circulation was formed after the obstacle near the inner wall of the channel. This new circulation may cause other undesirable effects and should be eliminated. To change this situation, the obstacle shape can be changed. A possible way to achieve this goal is to flatten part of the obstacle and diffuse the flow toward the wall. With this idea, the model was further revised as shown in Figure 20.

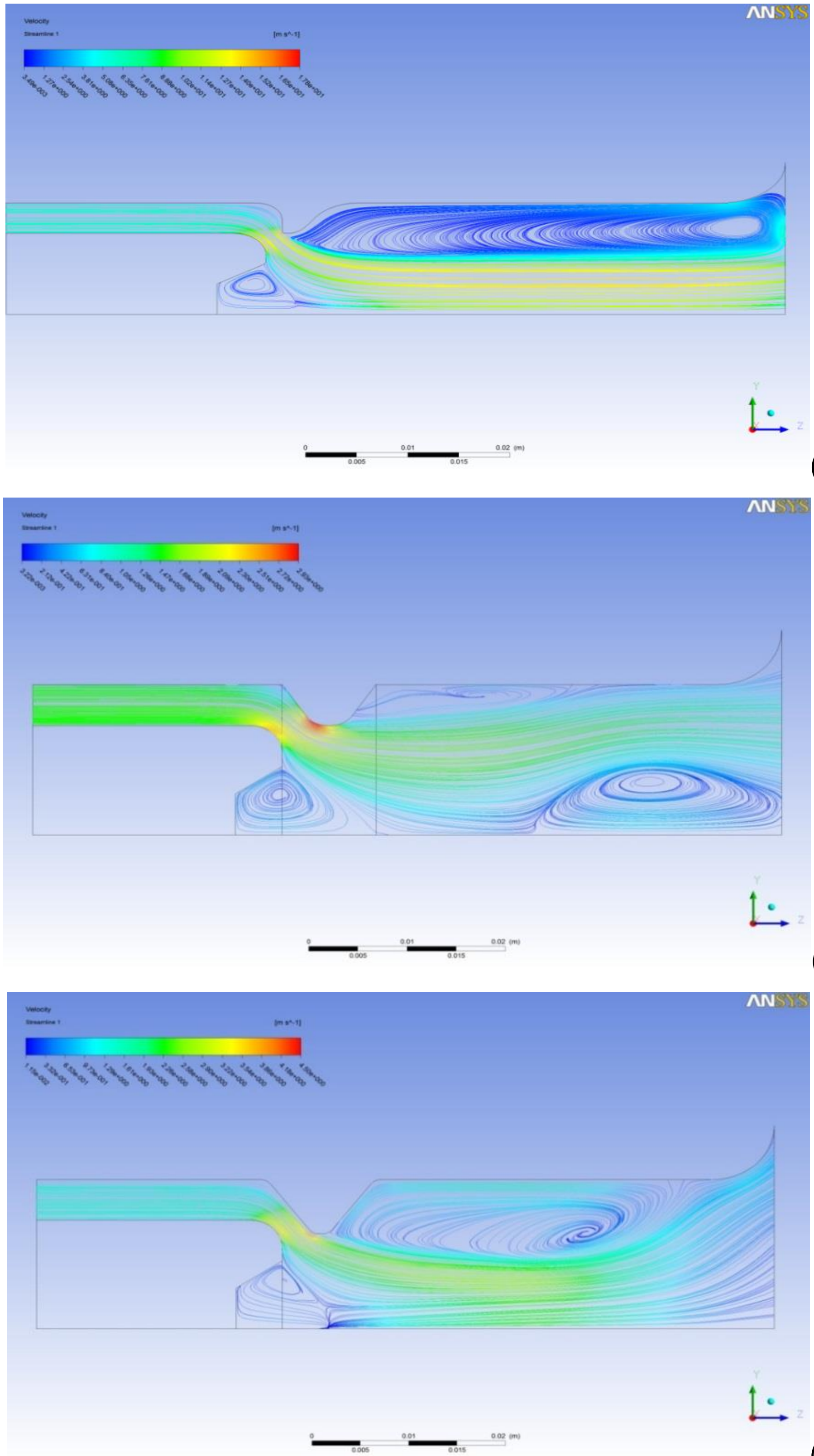

(a)
(b)
(c)

Figure 19. Models with taller obstacles on the inner wall of the flow channel

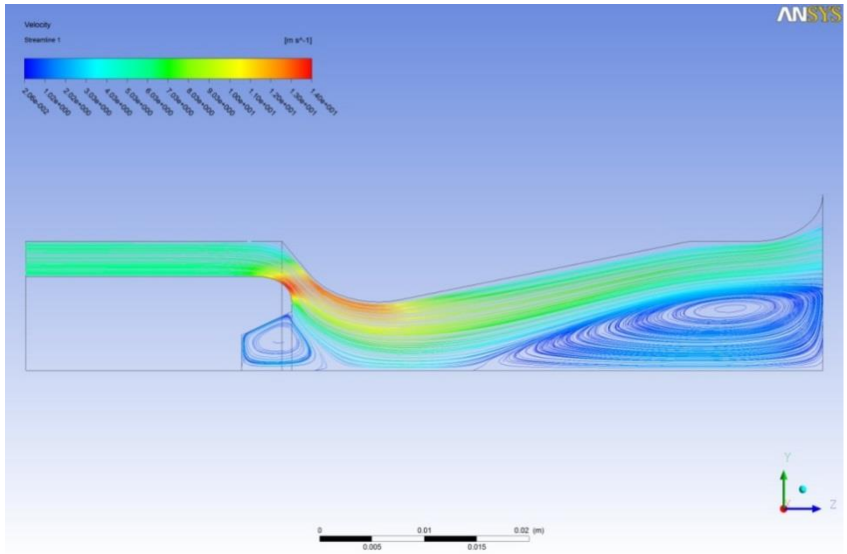

Figure 20. Optimized model based on Approach 2

Figure 20 shows the most promising solution to the dust deposition problem for the observation equipment to date. However, this numerical study does not include the flow domain in the combustion chamber, where the dust particles are actually located. Despite the fact that the flow conditions downstream (in the chamber) do not affect the flow domain in the channel in this model, the flow condition inside the chamber does have an effect on the boundary condition of the channel outlet. Also, the dynamics of the particles were not considered in this model. Particle motion is, for this model, simply assumed to be along the streamlines. However, the particle motion could be much more complicated.

The original system and the solution shown in Figure 20 were verified through experimental tests, and only then were further improvements considered.

Laboratory Testing of the Purging System

The optical window installed to view the combustion process in a coal gasification chamber is rendered inoperable after a period of weeks due to particulate from the combustion chamber being depositing onto the window. The reason for this particulate transfer is unknown; however, it is suspected that the flow characteristics of the nitrogen air stream, flowing into the combustion chamber from behind the optical window holder, are to blame. The prevailing theory of how particulates from the coal gasification combustion chamber are deposited onto the optical window is that a low pressure area in front of the optical window, created by an aerodynamic wake from incoming nitrogen, causes contamination to get pulled toward the window. This theory was initially developed through computational fluid dynamics (CFD) modeling of the flow in the optical channel where the optical window, and optical window holder, resides.

The experiment designed had two goals. The primary goal of the experiment was to determine the reasons for particulate transfer from the combustion chamber to the optical window. With a better understanding of the mechanism of particulate transfer, solutions can be developed to improve the design. In addition to determining the cause of deposits on the optical window the experiment needs to either verify or refute the CFD model.

If the CFD model is found to be incorrect it can be improved with added mechanisms to match the experimental results. With matching experimental and CFD results any proposed modifications can first be computationally modeled and the results can be considered reasonably accurate. This will allow a larger number of modifications to be made than would be possible with only the experimental design. The modifications producing the best results in the CFD model can then be fabricated and the results can be verified experimentally.

Experimental setup

The diagram of the experimental setup is shown in Figure 21. The tank (1) represents the coal gasification chamber of the actual design. The tank is not designed to handle either high pressure or high temperature; however, the dust filled environment was replicated in this experiment by agitating powdered chalk with a small fan (2). To filter the chalk out before the air exits into the exhaust system in the laboratory it is filtered using a 25 CFM_{max} air filter (3).

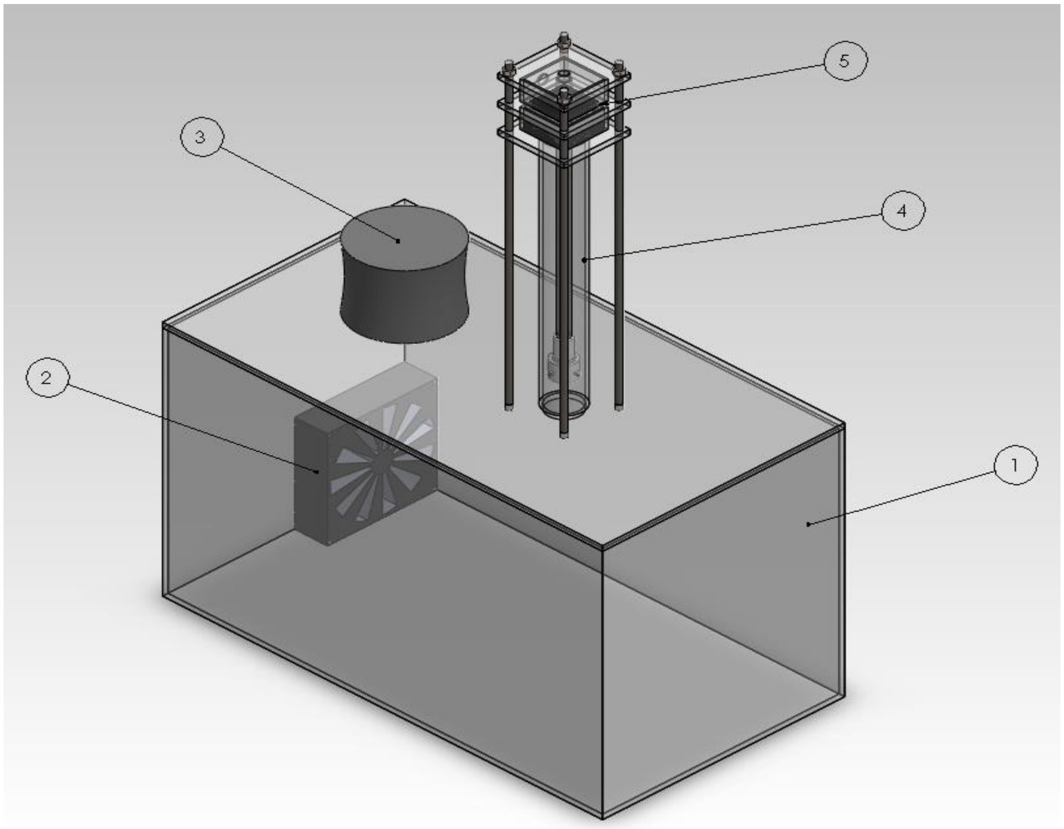

Figure 21. Diagram of the experimental setup for purging studies

The tube housing assembly (4) replicates the liquid cooled housing designed for the fiber-optics being used in the physical system. Inside this housing are a polycarbonate tube, nylon window holder, and glass window. These components allow a small flexible camera to be inserted into the system while keeping it sealed from the chalk dust being agitated by the airflow of the fan as well as the air coming down the tube housing. The window holder is threaded into place to allow easy replacement as new designs are developed.

Air enters the tube housing (4) from an air distribution assembly (5). The distribution assembly ensures that the air entering the system encounters the window holder uniformly around its surface. A photo of the experimental setup is shown in Figure 22.

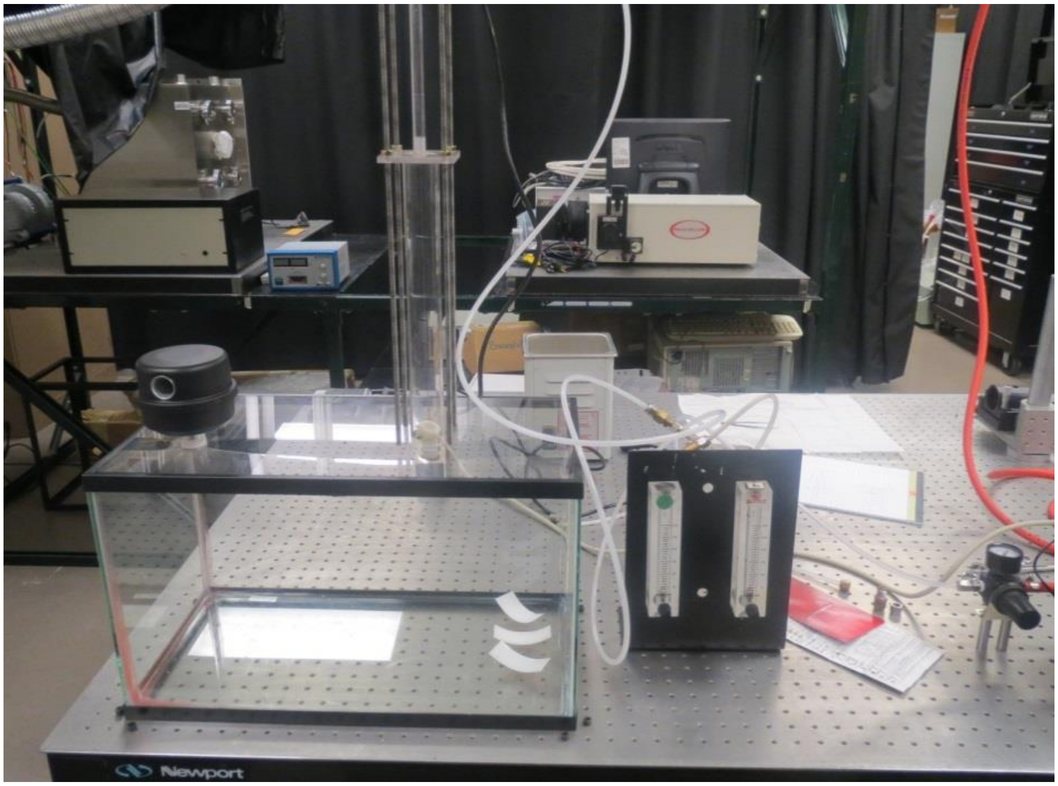

Figure 22. Photo of the experimental setup

Experimental procedure

The experiment limited the results to photo and video capture of the air flow as it passed between the optical window holder and the optical channel and entered the model combustion chamber.

The video results were very effective for comparison to the existing CFD model of the flow. Furthermore, the video allowed for the transition between laminar and turbulent flow to be observed. This transition was then verified by calculating the Reynolds number of the flow, serving as some evidence to the accuracy of the experiment, especially as it pertained to flow rate.

The photographic results, which are actually individual frames of the videos, effectively serve as examples of the generalized behavior observed at various flow rates. The actual behavior of the flow is very difficult to capture photographically.

As previously stated, the optical portion of the experiment is a scale model of the actual system and the tank has a volume of approximately 10 gallons and measures approximately 20 inches long, 11 inches deep, and 12 inches tall.

With this setup two different experiments were performed. The first filled the model combustion chamber with smoke, mimicking the particulate in the actual system, while clean air was introduced down the optical channel and past the optical window holder. This experiment required that the fan installed in the tank be used to distribute smoke throughout the chamber.

While the first experiment, using a smoke filled combustion chamber, was very effective in determining the flow rate necessary to completely clear the optical channel of contamination, the behavior of the clean air flowing into the channel past the window holder could not be observed. Seeing the behavior of this flow was necessary for proper analysis of the CFD model and of the mechanism of particulate transfer from the combustion chamber to the optical window. In order to make this incoming air stream visible a new experiment was devised in which the air in the combustion chamber would be kept stagnant and relatively clear and smoke would be introduced into the incoming air stream before it entered the optical channel. Using this technique the flow behavior as the air stream flowed between the window holder and the optical channel could be observed and this could be used to verify or refute the CFD model, to determine the laminar to turbulent transition flow rate and compare it to the calculated Reynolds number, and to determine the reason for particulate transfer, rather than simply the flow rates at which it does and does not occur.

Each of the two experiments described above, using a turbulent smoke-filled model combustion chamber, and using a stagnant clear chamber while introducing a smoke-contaminated air stream, effectively followed the same procedure.

The behavior of the flow within the optical channel from the window holder to the entrance to the model combustion chamber was filmed using a Panasonic DMC-TZ1 digital camera. During the filming the flow rate was gradually increased from 0 to 2.0 SCFM for the contaminated chamber experiment and from 0 to 1.0 SCFM for the contaminated air stream experiment. In both cases the area of interest was illuminated using a JDS Uniphase Model 1135P laser powered by a JDSU Model 1216-1 power source with external light eliminated by performing the experiment underneath an optical black-out cover. The flow rate of the incoming air was measured using a Dwyer Instruments VFB-90-SSV Flowmeter.

Individual frames of these films were used to, as necessary, show the generalized flow behavior at specific flow rates. In addition to the photographic results the Reynolds number of the flow between the optical window holder and the optical channel was calculated. Furthermore the velocity of the flow at this point was also determined in 0.1 CFM intervals.

The Reynolds number calculation, with numbers below 2100 being laminar, between 2100 and 4000 being transitional, and above 4000 being turbulent, was used to verify the accuracy of the flow rates measured in the experiment. With the experimental data (video) verified with the Reynolds number calculations the calculations for air velocity could then be assumed, with reasonable certainty, to be accurate.

Experimental testing of the original design

Experimental results are presented in Table 1 as well as in Figure 23 and Figure 24. The view on Figure 23(a-d) and Figure 24(a-d) represents the bottom part of the tubing housing (4), shown on Figure 21. Using the flow rate measurements from the Dwyer Instruments Flowmeter, along with the dimensions of the optical channel and optical window holder, the local Reynolds number of the air stream as it passes between the window holder and the channel wall can be calculated as:

$$\mathrm{Re} = \frac{UD_H}{\nu} \quad (1)$$

where U is the average velocity of the flow, D_H is the hydraulic diameter of the system at the point of interest, and ν is the kinematic viscosity of the fluid. The average velocity of the flow is calculated as

$$U = \frac{Q}{A} \quad (2)$$

where Q is the measured volume flow rate and A is the cross-sectional area of the annulus created by the optical window holder and the optical channel. For an annulus the hydraulic diameter is

$$D_H = D_o - D_i \quad (3)$$

where D_o and D_i are, respectively, the outer and inner diameters. In the case of this experiment the outer diameter is the diameter of the optical channel while the inner is the outside diameter of the optical window holder.

Table 1. Measured flow rate, calculated flow rate, calculated maximum average velocity, and local Reynolds number. The kinematic viscosity of air was taken to be 1.57 10^{-2} cm^2/s.

Measured Flow Rate ($SCFM$)	Flow Rate ($\frac{cm^3}{s}$)	Velocity ($\frac{cm}{s}$)	Reynolds Number
0.0	0	0.00	0.00
0.1	47.2	10.5	635
0.2	94.4	20.9	1270
0.3	142	31.4	1910
0.4	189	41.8	2540
0.5	236	52.3	3180
0.6	283	62.7	3810
0.7	330	73.2	4450
0.8	378	83.7	5080
0.9	425	94.1	5720
1.0	472	105	6350
1.1	519	115	6990
1.2	566	125	7620
1.3	614	136	8260
1.4	661	146	8890
1.5	708	157	9530
1.6	755	167	10200
1.7	802	178	10800
1.8	850	188	11400
1.9	897	199	12100
2.0	944	209	12700

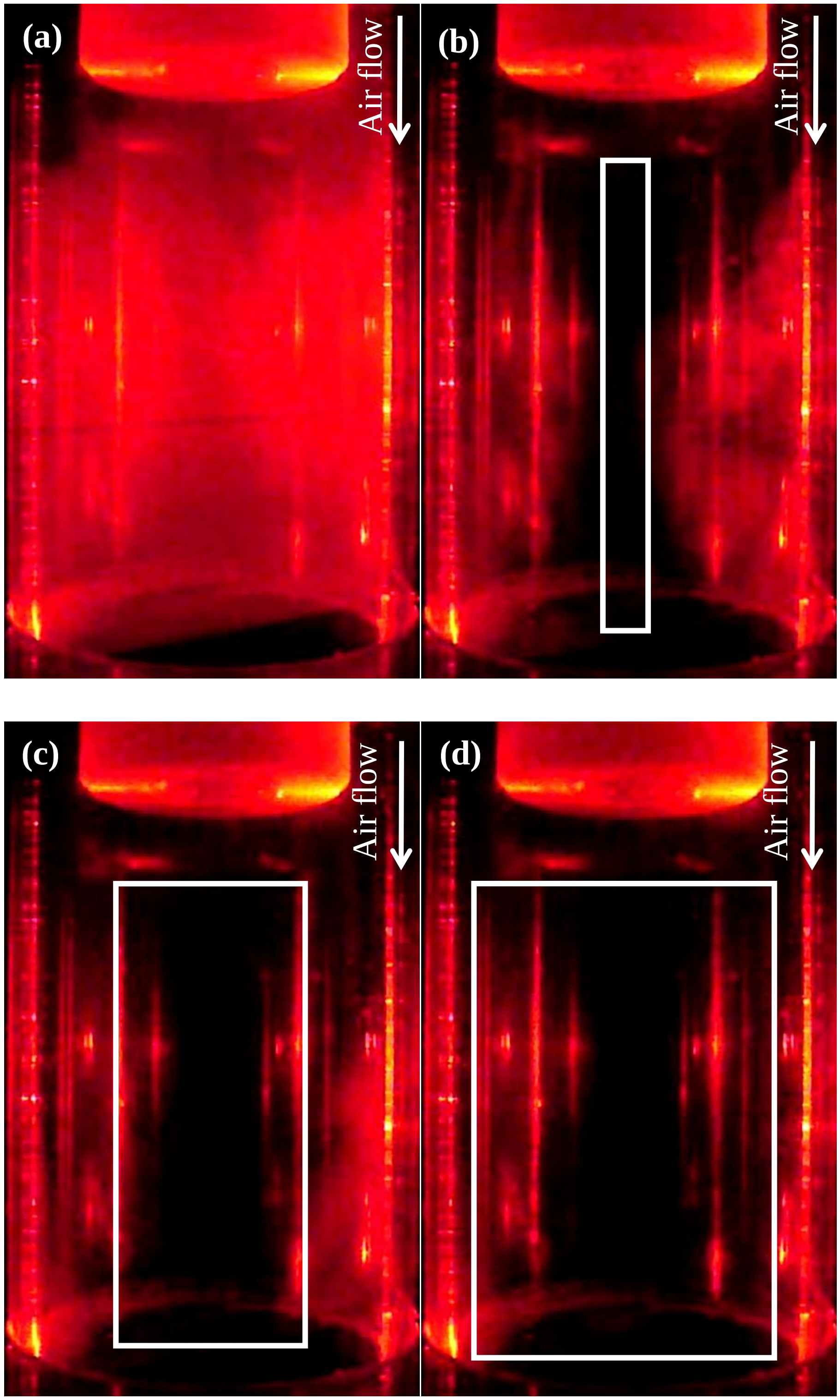

Figure 23. Photographic results of turbulent combustion chamber experiment. Flow rates of (a) 0.0 SCFM, (b) 0.8 SCFM, (c) 1.2 SCFM, and (d) 2.0 SCFM. Highlighted box shows area free of combustion chamber contamination.

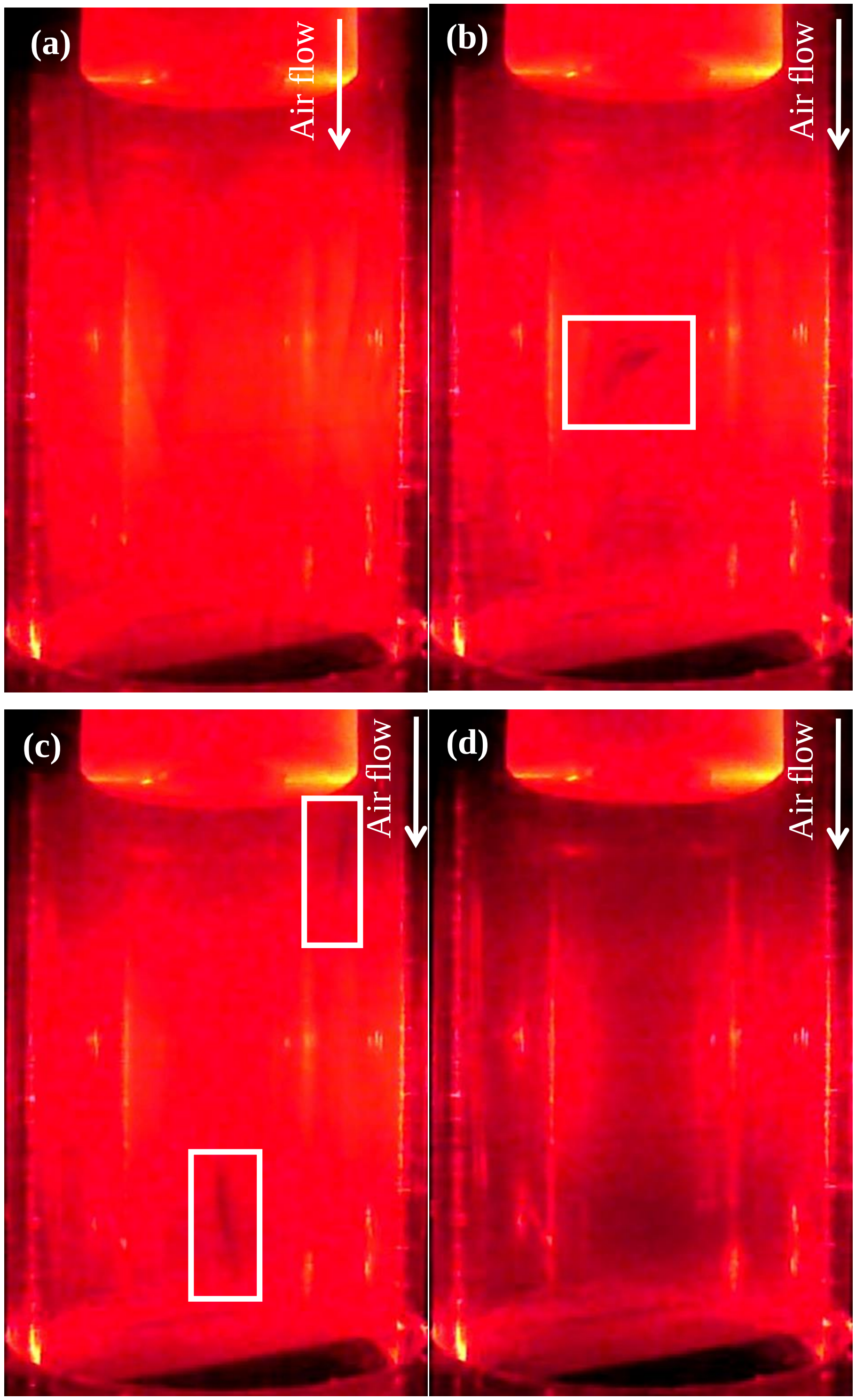

Figure 24. Photographic results of stagnant combustion chamber experiment. Flow rates of (a) 0.2 SCFM, (b) 0.4 SCFM, (c) 0.6 SCFM, and (d) 0.8 SCFM. Boxes highlight combustion chamber gas penetration into optical channel.

For this experiment the air stream temperature was considered relatively constant and the velocity of the flow was consistently small enough to neglect any changes in air density. Therefore, the kinematic viscosity was considered a constant.

The calculation of the Reynolds number allows the flow to be characterized as laminar($Re \leq 2100$), transitional($2100 < Re < 4000$), or turbulent($Re \geq 4000$). However, during the first experiment there were actually two air streams present and mixing in the optical channel. Obviously one air stream is the intended air being introduced to the system. The second air stream is generated due to the turbulence being created in the smoke-contaminated model combustion chamber. In fact the combustion chamber air stream was found to be so turbulent that laminar flow never actually existed in the optical channel. Therefore, the Reynolds number calculations for the first experiment are not indicative of the actual flow characteristics. However, this was one of the primary reasons the second experiment was performed.

By introducing smoke to the incoming air stream the air in the chamber could remain stagnant. This effectively eliminated the air stream mixing effect that was observed in the first experiment. Furthermore maintaining a stagnant model combustion chamber allowed laminar flow to be achieved within the optical channel. With this second experiment the Reynolds numbers shown in Table 1 closely match the video results obtained experimentally. The flow is laminar at low flow rates with the laminar to turbulent transitioning occurring around 0.4 or 0.5 SCFM. This serves as evidence that, for the stagnant chamber test, the Reynolds numbers calculated using the above equations are indicative of the flow behavior in the area between the optical window holder and the optical channel wall.

Experiment #1, using a model combustion chamber filled with smoky turbulent air, most closely matched the circumstances of the actual coal gasification optical system. Figure 23(a-d) shows the effect the incoming clean air stream had on removing particulate from the area in the optical channel near the optical window.

Obviously at a flow rate of 0.0 SCFM of flow Figure 23(a) the entire area in front of the optical window was contaminated with smoke. At a flow rate of 0.8 SCFM the area in front of the window began to open up slightly. This is highlighted in Figure 23(b). Increasing this flow rate to 1.2 SCFM cleared most of the smoke out of the optical channel (Figure 23c). By approximately 2.0 SCFM (Figure 23d) the entire optical channel was clear of smoke. As in Figure 23(b), the area clear of smoke-contamination is highlighted in Figure 23(c) and Figure 23(d).

The images shown in Figure 23(a-d) do not, however, give a true indication of the behavior of the flow in the optical channel. The video results show that, at small flow rates (0.1-0.6 SCFM), the clear air stream was not substantial enough to remove the smoke from the optical channel. However, with flow rates large enough to create a complete path of clean air all the way to the model combustion chamber, small amounts of smoke would penetrate the clean air stream and reach the optical window. This smoke penetration was believed to be caused by the wake created by the optical window holder. The theory being that this low pressure wake was pulling contamination to the optical window. A new experiment was devised to determine if there was, as suspected, a low pressure area in front of the optical window that was causing particulate transfer from the combustion chamber.

In Figure 23(a-d), the incoming air stream exists anywhere that the smoke does not. However, the behavior within this clear air stream could not be directly viewed. To view this air stream it was decided that, for the second experiment, the incoming air would be injected with smoke while the model combustion chamber would be full of clean air.

In addition to the need to view the flow behavior of the incoming air stream to confirm the existence of a low pressure wake, the second experiment needed to be performed so that laminar flow could be achieved within the optical channel. Achieving laminar flow in the air stream necessitated that the combustion chamber air be left relatively stagnant. It was found in the first experiment that the turbulent nature of the air within the chamber prevented the flow within the optical channel from being laminar, regardless of supposed Reynolds number of the flow. Generating laminar flow allowed for a comparison between experimental results and existing CFD models of the system.

The CFD models show the time averaged flow behavior of the incoming air stream – effectively time averaged streamlines for the flow. This type of time averaged data could not be accurately captured on video. However, generating laminar flow allowed for the general behavior of the incoming air stream to be seen as it passed between the optical window holder and the optical channel wall. This flow behavior, at flow rates small enough to achieve laminar flow, was very similar to the time averaged behavior shown in CFD models of much higher flow rates. This was an indication that the CFD models did capture the general flow behavior, at least for small experimental flow rates. It could only be assumed however, that the behavior of the laminar flow that existed at relatively small flow rates would be similar to the time averaged behavior of the flow when higher flow rates caused the air stream to become turbulent.

Figure 24(a-d) shows selected images from the stagnant chamber experiment. Figure 24(a) shows the flow at 0.2 SCFM. While it is difficult to see in the image, the video of the experiment very clearly shows that, at this flow rate, the flow is laminar, as predicted by the Reynolds number calculation. This was seen because the incoming smoky air stream did not readily mix with the clean air in the optical channel and the combustion chamber and these two separate air streams generated streamlines of the flow. It is these streamlines that were compared to the CFD models of the flow and allowed for determination that, at least for laminar flow situations, the CFD model is accurate.

As for the original problem of particulate from the combustion chamber rendering the optical window unusable, 0.2 SCFM was found to be too small a flow rate to eliminate this problem. This is evidenced simply by the existence of streamlines in the flow. As stated, the streamlines only exist because the two air streams (stagnant clear air and incoming smoke-injected air) do not readily mix. Therefore the existence of the streamlines is evidence that air from the combustion chamber must still be present in the optical channel near the optical window.

Also of interest in Figure 24(a) is that the streamlines, especially in the video, show evidence of a significant wake being created by the optical window holder. This wake is the low pressure area that was suspected in the first experiment of causing contaminated gases to enter the optical channel and reach the optical window, rendering it unusable. However, because the flow is still laminar in Figure 24(a) the actual transfer of combustion chamber gases was not observed. Instead the flow rate was so small (0.2 SCFM) that the combustion chamber gases had yet to be sufficiently displaced from the optical channel.

Once the flow rate was increased to 0.4 SCFM (Figure 24b) the flow began to become more turbulent and the streamlines created by the clean combustion chamber air disappeared. However, highlighted area in Figure 24(b) is the first sign of the suspected mechanism of transfer of particulate to the optical window. As suspected during the first experiment, and confirmed by the laminar flow portion of the second experiment, a low pressure area, created by the wake of the window holder, exists in front of the optical window. When the incoming flow is substantial enough to force combustion chamber gases out of the optical channel, the low pressure area in front of the window tends to periodically pull small amounts of contamination to the optical window. This occurs even though the flow within the optical channel is, effectively, turbulent. A small amount of combustion chamber air is highlighted in Figure 24(b). The video results clearly show this contamination getting pulled into the optical channel from the combustion chamber and up to the optical window. Even though this transfer of gases is only periodic it could be enough, over time, to render the optical window in the actual system inoperable.

Increasing the flow rate to 0.6 SCFM (Figure 24c) shows a new problem developing as it pertains to the transfer of combustion chamber gases to the optical window. It can only be assumed at this flow rate that, at least to some degree, a low pressure area still exists in front of the optical window. This low pressure area, however, seems to have become secondary at this increased flow rate.

Conservation of mass shows that for more air flow to pass between the constant geometry optical channel and optical window holder, the velocity of the flow must increase. Furthermore, the Bernoulli principle indicates that as this velocity increases the pressure must decrease. The low pressure that now exists between the optical window holder and the optical channel wall is, at this flow rate, the primary mechanism of combustion chamber particulate transfer. Figure 24(c) shows two instances of this combustion chamber gas transfer. Each is highlighted by a white box. Essentially at this flow rate (0.6 SCFM) the particulate is pulled from the combustion chamber, up the center of the optical channel to the tail of the optical window holder wake, and then up to the area between the optical window holder and the channel wall. This is a very significant problem, possibly more significant that the issues observed using the turbulent combustion chamber or using the stagnant combustion chamber at transitional flow rates ($2100<Re<4000$). The problems observed previously involve particulate getting pulled to the optical window, rendering it unusable. In both of the previous situations it seemed that this would happen in some set amount of time. However, with particulate now getting pulled toward the outer edge of the optical window holder the problem is two-fold.

Obviously the problem of particulate from the combustion impinging itself on the surface of the optical window still exists. Additionally a problem exists where the area between the optical window holder and the channel wall is gradually being reduced by the same transfer of contaminated material. The reduction of this area will cause the flow velocity to increase and subsequently the pressure in this area will decrease. This pressure decrease will cause more particulate to get pulled toward the optical window more quickly than if the area between the window holder and the channel wall remained constant. Effectively, with particulate getting pulled toward the outer edge of the optical window holder not only will the optical window become inoperable, but it will likely happen more quickly than it would if the combustion chamber material were getting pulled directly to the optical window. Increasing the flow rate further, however, seemed to lessen the frequency of particulate transfer.

Figure 24(d) shows the results of the stagnant model combustion chamber experiment at an incoming air flow rate of 0.8 SCFM. This image shows no evidence of particulate transfer to the optical window. This is not, however, entirely indicative of the flow behavior at higher (0.8-1.0 SCFM) flow rates. At these higher flow rates there were still instances of particulate transfer very similar to the results shown in Figure 24(c). However, increasing the flow rate from 0.6 SCFM to 0.8 SCFM reduced the frequency of this particulate transfer. No flow rate was achieved, however, that completely eliminated this transfer phenomenon. The obvious conclusion from this is that the effect increasing the flow rate has on displacing the combustion chamber gases is more significant than the effect the associated pressure drop created between the window holder and the channel wall has on contamination transfer. However, because this transfer mechanism was never completely eliminated there must be a point of diminished returns where increasing the flow rate no longer has an effect on the amount, or the frequency, of particulate transfer from the combustion chamber. Furthermore, even though the frequency of this particulate transfer was dramatically reduced, it was still far too frequent to solve the problem occurring in the actual optical system.

With the effects of flow rate on combustion chamber material transfer thoroughly investigated, and with a substantial knowledge of the effect the optical window holder has on the incoming air stream flow, the next course of action was to install flow obstructions in the optical channel downstream of the incoming air flow. The idea of these obstructions is two-fold. Primarily they exist to reduce or eliminate the low pressure wake created by the optical window holder by diverting the flow of the incoming air stream to the area immediately in front of the optical window. Secondarily, however, they must not impede the incoming air flow in such a way that new low pressure areas substantial enough to generate particulate transfer are created.

With a turbulent combustion chamber it was found that a larger incoming air flow rate was necessary to displace contaminated gasses from the optical channel. In fact the flow rate necessary to remove contaminated air from the optical (1.5-2.0 SCFM) was approximately twice that required to displace the contamination when the air in the combustion chamber was stagnant (0.8-1.0 SCFM). However, changes in flow rate were not found to be enough to completely prevent particulate transfer from the combustion chamber to the optical window.

The shape of the optical window holder was found to create a significant wake in the incoming air stream. This low pressure wake tended to periodically pull contamination from the combustion chamber to the optical window. The frequency of this periodic transfer was decreased by increasing the flow rate, however, regardless of flow rate, the problem was never completely eliminated. Additionally, increasing the flow rate, especially with a stagnant combustion chamber, created an additional low pressure area that also pulled particulate from the combustion chamber back into the optical channel. This low pressure area existed between the optical window holder and the optical channel wall and was created by the increased air velocity necessary at increased flow rates.

This second low pressure area, which was predominantly observed using a stagnant combustion chamber, though it is suspected that the same phenomenon existed with a turbulent combustion chamber, produced an additional problem. When the flow rate was large enough that this second low pressure area existed, and when this new low pressure area reached a pressure lower than that of the wake created by the optical window holder, the new low pressure area became the primary mechanism of material transfer. At this point not only would the particulate being transported block the view through the optical window but it would begin to reduce the area between the window holder and the channel wall, thus speeding up the contamination transfer process.

The CFD models did not, however, indicate that the pressure in the area between the window holder and the channel wall were ever less than the pressure within the wake created by the window holder, even up to flow rates of 6.0 SCFM. This is one area where the experimental results could serve to create better CFD models of the system because the video results from the stagnant chamber clearly show the combustion chamber gases being transferred to the edge of the optical window holder. This type of transfer would only occur if the pressure at that edge of the optical window holder were lower than the pressure in the immediate vicinity of the optical window.

The experiments, particularly the stagnant chamber experiment, did confirm the CFD model as it pertained to the existence of a wake created by the optical window holder. Furthermore, the CFD models indicate that flow circulation existed within this wake and this, as observed in the experiments, causes contaminants from the combustion chamber to become trapped in the immediate vicinity of the optical window.

With a few necessary changes to the CFD model to make it match the experimental evidence, proposed changes to the optical channel can first be modeled to see if they achieve the desired results before the changes are made to the experimental system. At this time the goal of any proposed changes is to reduce or eliminate the wake created by the optical window holder while not creating new, and potentially problematic, areas of low pressure.

Experimental testing of the modified design

Two configurations of the optical channel obstruction were designed, manufactured and tested experimentally. These configurations are shown in Figure 25 and Figure 26.

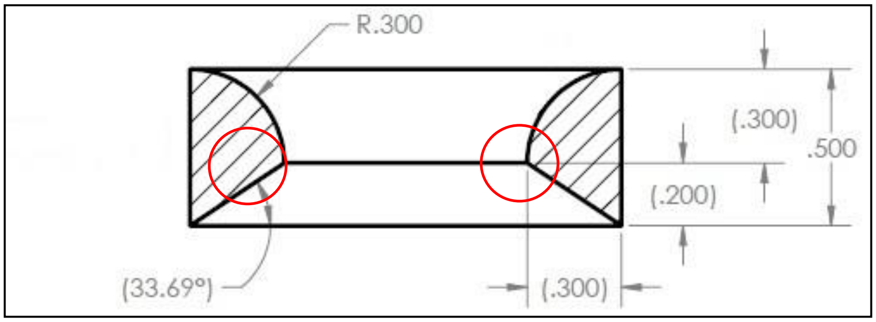

Figure 25. Dimensioned drawing of experimental Obstruction 1

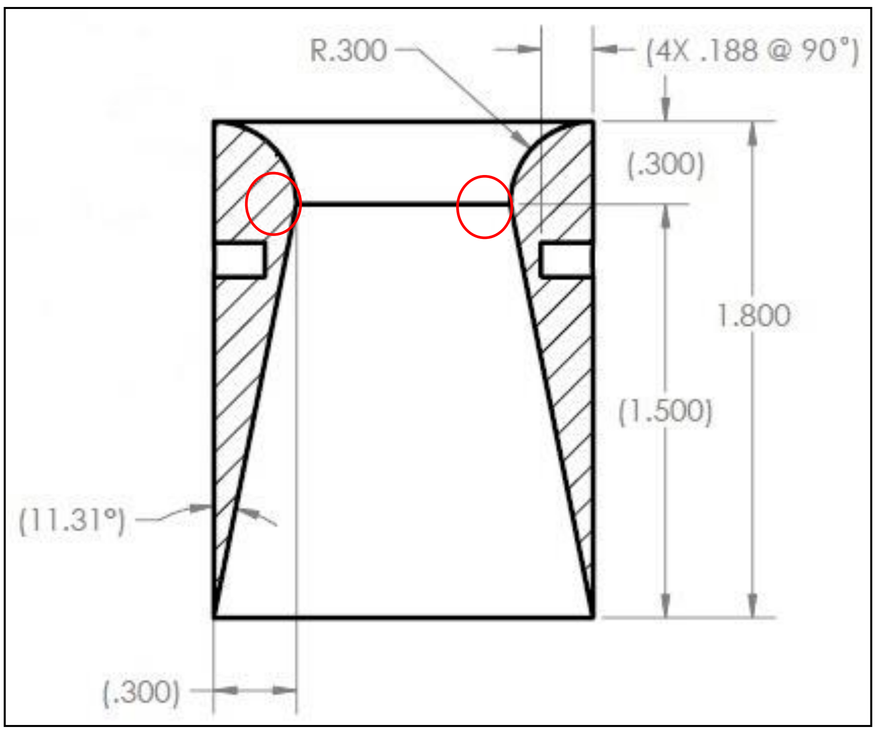

Figure 26. Dimensioned drawing of experimental Obstruction 2

The obstructions were introduced in the vertical flow tube of the experimental setup. The tests were performed with air flows saturated with smoke particles. The setup was illuminated by a laser beam to visualize the flow behavior.

Figure 27(a-e) show the general flow characteristics at the indicated flow rates obtained with Configuration 1.

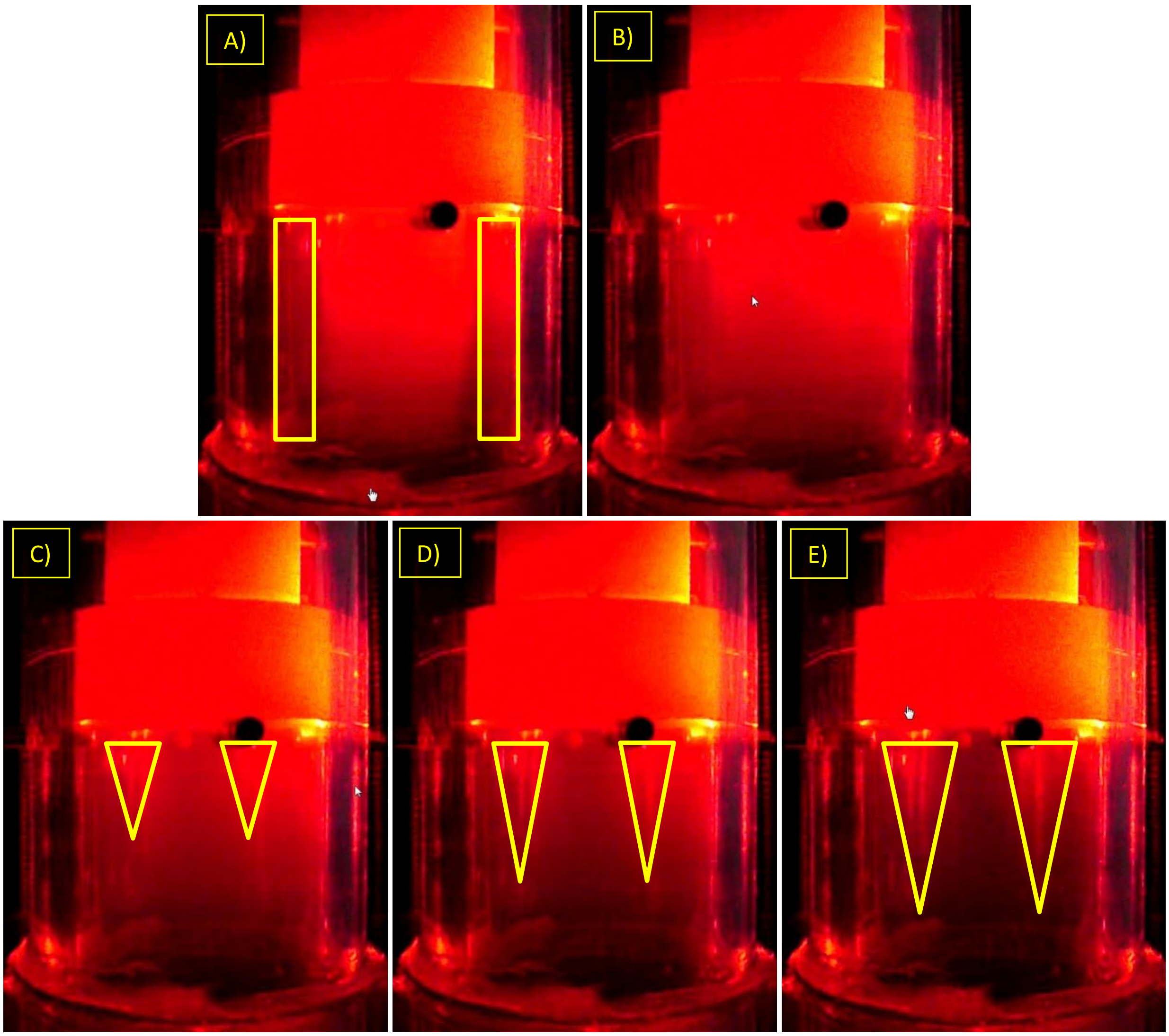

Figure 27. Experimental images of the flow in the optical channel modified using the obstruction with Configuration 1: (a) 0.1 SCFM, (b) 0.2 SCFM, (c) 0.4 SCFM, (d) 0.5 SCFM, (e) 0.7 SCFM.

At very low flow rates (< 0.1 SCFM), as highlighted in Figure 27(a) there is no incoming air flowing near the walls of the optical channel beyond the obstruction. Figure 27(b) shows that even at flow rates as small as 0.2 SCFM the incoming air completely fills the optical channel and flows into the model combustion area in a laminar fashion. Beginning at a flow rate of approximately 0.4

SCFM an area of turbulence begins to develop at the transition between the radius of the obstruction and the exit diffuser. This is highlighted in Figure 27(c). The turbulence at this location continues to grow up to the maximum flow rate tested (1.2 SCFM). Figure 27(d, e) show the size of this area at 0.5 SCFM and 0.7 SCFM, respectively. Figure 25 shows a cross-section of the obstruction used for the experiment with the transition that created the turbulence highlighted. One important note is that this transition effect is greatly reduced in the configuration with Obstruction 2. This is due to the fact that Obstruction 2 is considerably taller than Obstruction 1. Configuration 2 was not used for imaging due to the necessity of an unobstructed view to observe the flow behavior.

We believe that, if the proposed obstruction is used, the turbulent eddies observed and shown in Figure 27(c-e) would be eliminated, or at least greatly reduced. Furthermore, comparing these results to the various changes that were made to the optical window holder shows the obstruction with Configuration 2 to be a far superior technique to eliminating undesirable eddy patterns within the optical channel. While there may be ways to further optimize this design, placing an obstruction of this type between the optical window holder and the combustion area has thus far proven to be the most effective method of preventing contamination of the optical window.

Design Modifications

The results of the modeling revealed that the high velocity purging flow around the original optical window assembly (Figure 28) generated gas recirculation (Figure 29) resulting in particulate transfer to the surface of the optical window. The modeling results were confirmed experimentally (Figure 30).

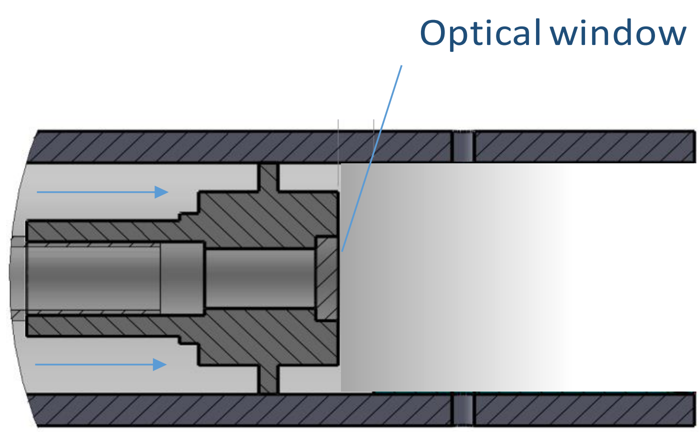

Figure 28. Original design of the optical window assembly

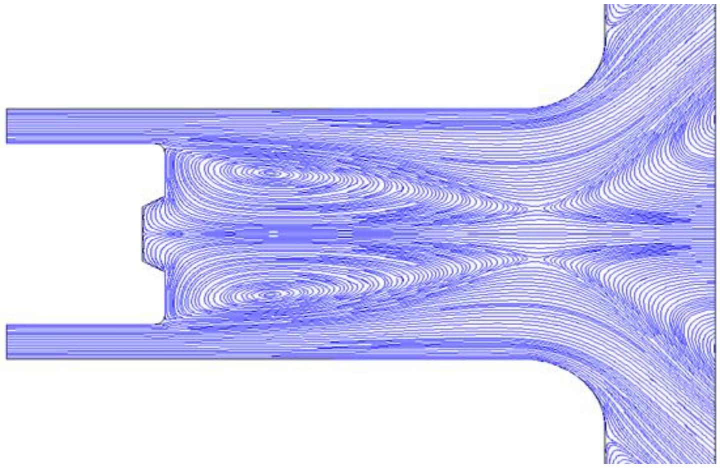

Figure 29. Numerical simulation of the nitrogen purging flow around the original window assembly

Figure 30. Visualization of the purging flow around the original window assembly

The project team developed a modified design of the probe. The modification involves placing an obstruction in the optical channel in front of the window as shown in Figure 31. The redesigned configuration was tested numerically and experimentally. The results of the numerical (Figure 32) and experimental (Figure 33) studies confirmed that the modification of the probe will significantly reduce or eliminate the particulate entrainment into the purging channel and their deposition on the optical window.

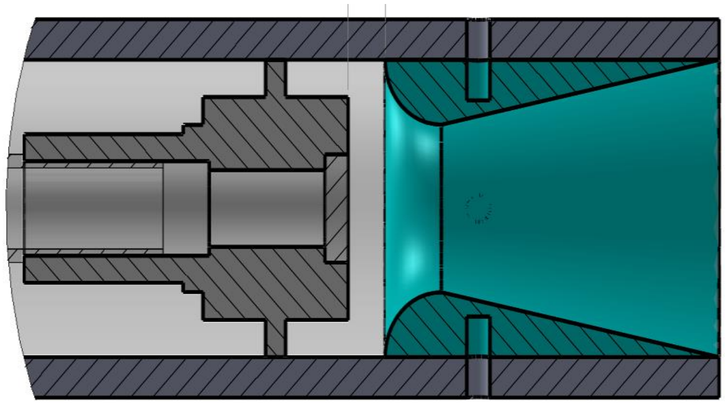

Figure 31. Modified design of the nitrogen purging channel

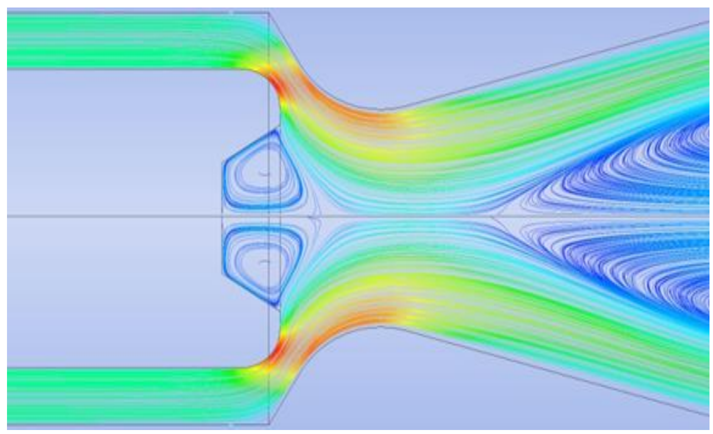

Figure 32. Numerical simulation of the nitrogen purging flow around the modified window assembly

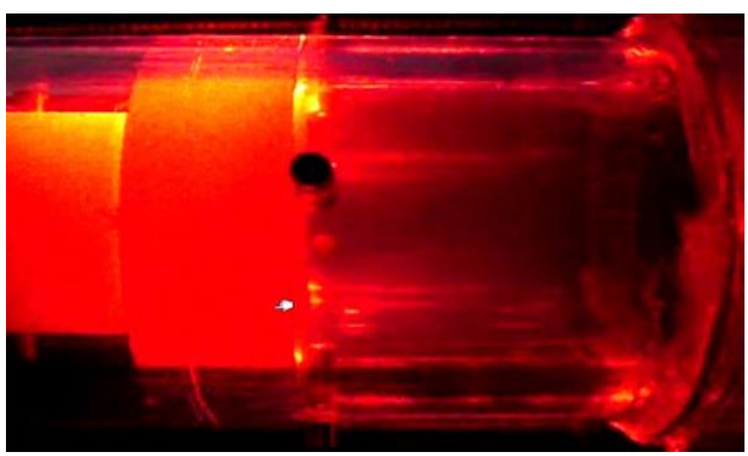

Figure 33. Visualization of the purging flow around the modified window assembly

The proposed modification did not alter the optical field-of-view of the sensor.

Task 4.0 Sensor Modification and Installation at the Wabash River Gasifier

Figure 34 shows a schematic of the sensor installation at the Wabash River gasifier. The flame image collected by the fiber-optic probe (FOP) is transmitted through a 30-foot long fiber-optic bundle to a sensor station. The second is collected by the digital video camera, then simultaneously displayed and recoded on the data acquisition computer. The sensor station was installed in the direct vicinity of the gasifier. The enclosure was designed to protect the sensor equipment from seasonal temperature variations and coal dust and should allow short-term operator access and maintenance. Long-term monitoring is possible by connecting remotely to the sensor station over an Ethernet line.

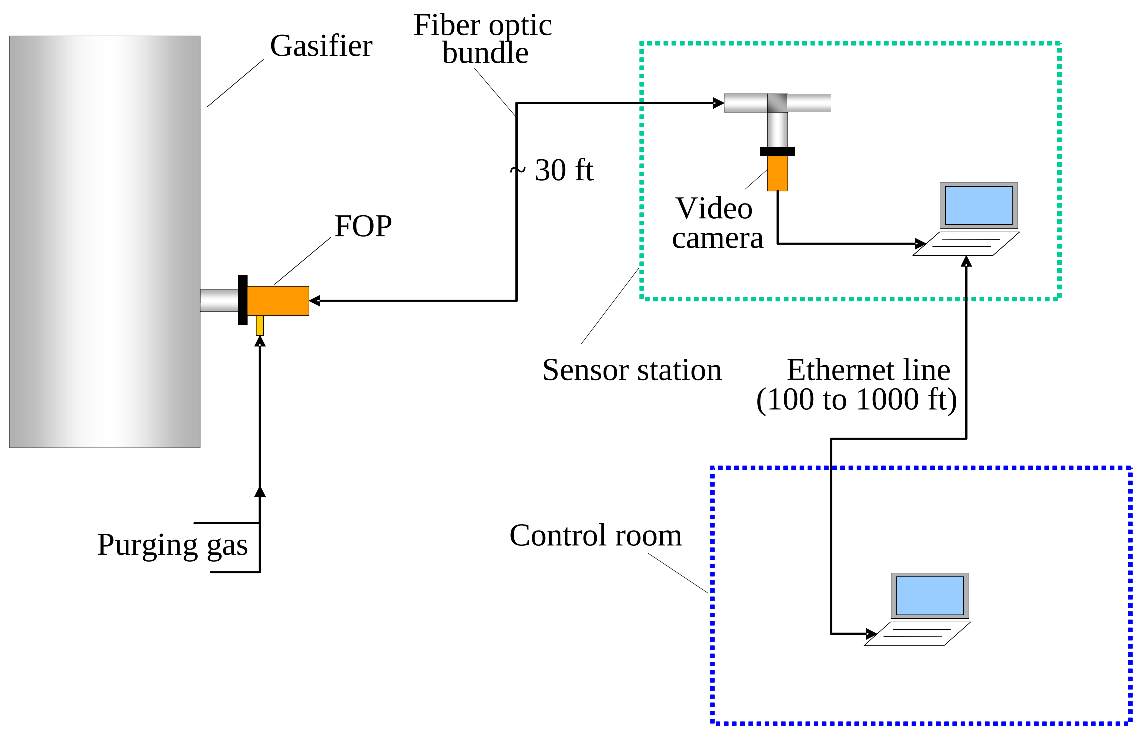

Figure 34. Schematic of Sensor Installation at Wabash River Gasifier

Figure 35 shows a schematic of the water cooled fiber-optic probe (WCFOP). The WCFOP consists of a water-cooled, nitrogen-purged enclosure and fiber-optic bundle encased in a protective 1/4" stainless steel sleeve with a sapphire window assembly welded at the front end of the sleeve. The bundle enclosure is expected to withstand temperatures and pressures exceeding 550 psig and 600 °F, respectively.

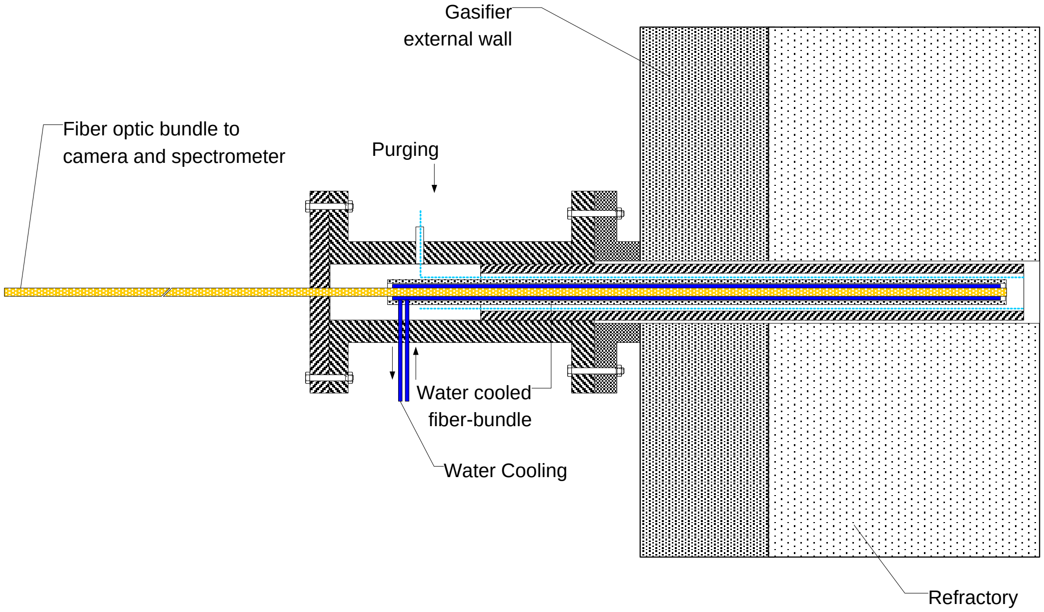

Figure 35. General schematic of the water cooled fiber-optic probe

The sensor was assembled and installed at the Wabash River gasifier by the CB&I representatives with the support of GTI personnel. The assembly included the optical probe incased in the water cooled/nitrogen purged nozzle, a light sensor (color digital video camera), and a data acquisition system. The probe was connected with the camera with a 30 foot long fiber optical bundle. A photograph of the probe assembly is shown in Figure 36.

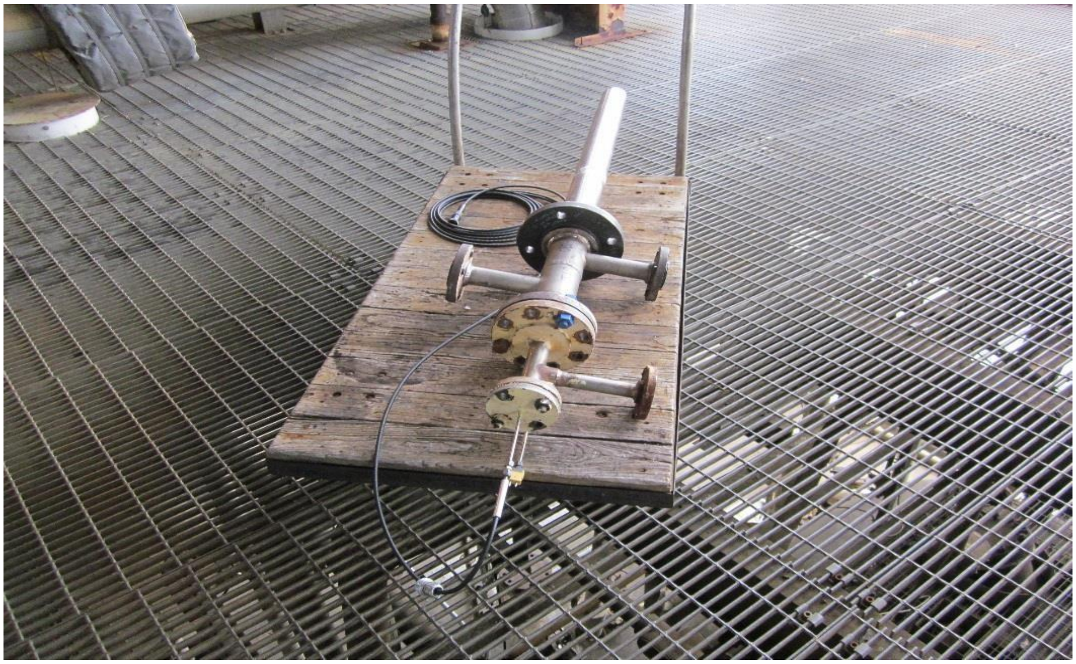

Figure 36. Probe assembly

The water cooled sensor probe was installed at the same location as the one used to access the gasifier temperatures under the previous project (Figure 37). The sensor camera and the data acquisition computer were placed in the specially designed nitrogen cooled enclosure installed near the gasifier.

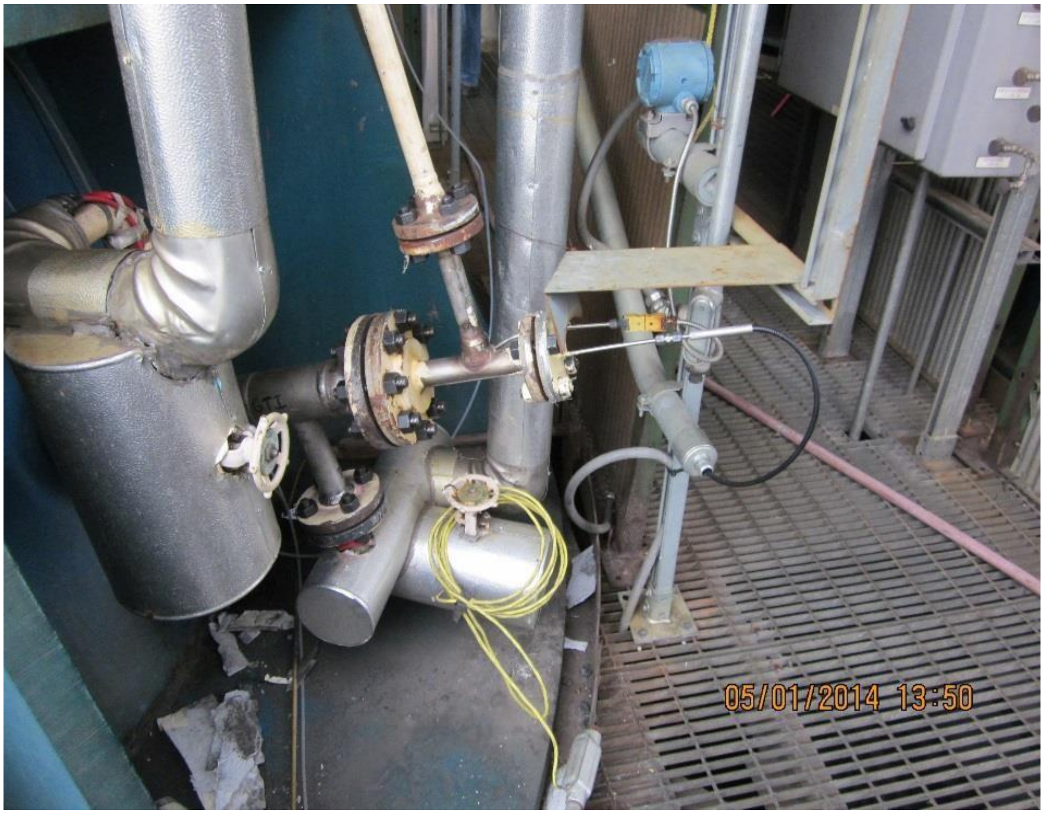

Figure 37. Installation location

Task 5.0 Sensor Testing at the Wabash River Gasifier

Maintaining unobstructed optical access

One of the biggest challenges faced during the prior sensor testing at the Wabash gasifier conducted under the previous project was maintaining the optical access open. At that time, the project team was not able to sustain unobstructed view of the gasifier for a period longer than six weeks due to the contamination of the probe's sapphire window with fine black particles (Figure 38).

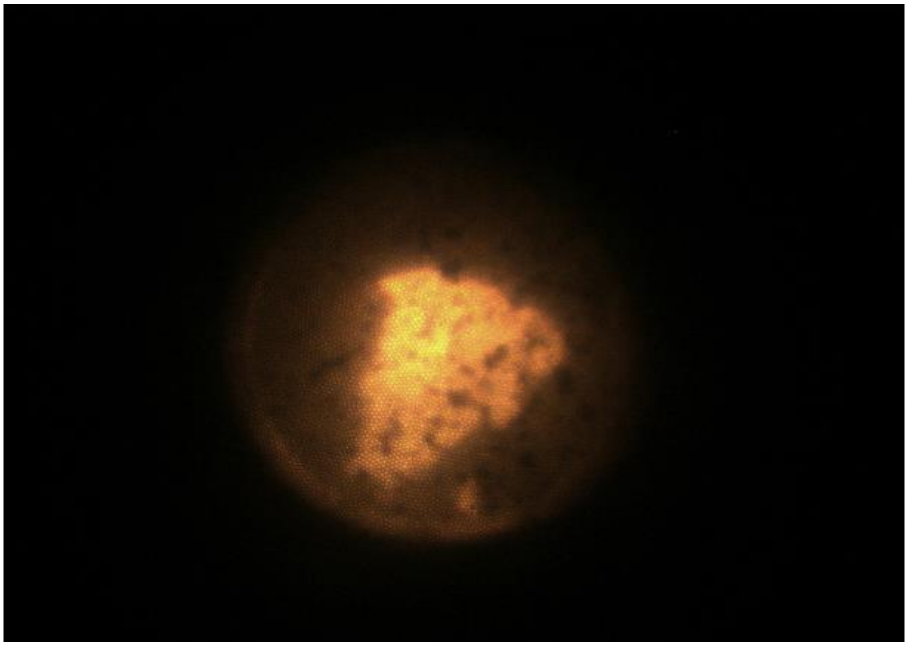

Figure 38. Sapphire window condition (Original design) after 5 weeks of testing under the previous project

The field testing, completed under the current project to date, showed no particulates deposition on the sapphire window (Figure 39).

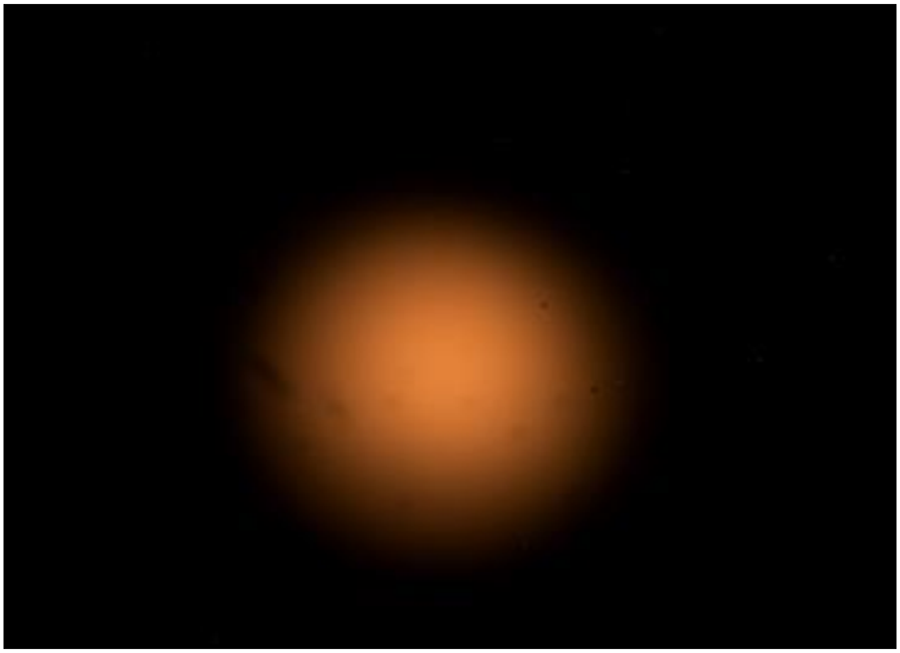

Figure 39. Sapphire window condition (Redesigned window assembly) after 14 weeks of testing conducted under the current project

Performance of the Gasifier Sensor software during the first two months of testing

The project team developed the Gasifier Sensor software which allowed the real time processing and storage of imaging data obtained by the gasifier probe. The testing showed that developed software was capable of collecting the gasifier images and translating the emitted light intensity into temperature in real time. The software records attained the temperature as well as the raw data (video images of the gasifier). The user could select the temperature averaging and recording intervals. The software automatically adjusted the camera's exposure time to maximize the signal-to-noise ratio and to prevent saturation of the camera's detectors. During the early stage of the current testing incorrect software settings caused periodic saturation of the camera's sensor and, as a result, produced some faulty temperature readings. The camera settings were modified and the issue was resolved. No erroneous readings were observed since the modification of the software settings was completed.

Temperature monitoring results

The graph below (Figure 40) shows comparison of the gasifier temperature acquired with the GTI Gasifier sensor and the thermocouple reading during the preheating of the gasifier utilizing a natural gas burner prior to switching to the slurry operation. The thermocouples could not be used during the regular slurry operation due to the high temperature corrosive environment.

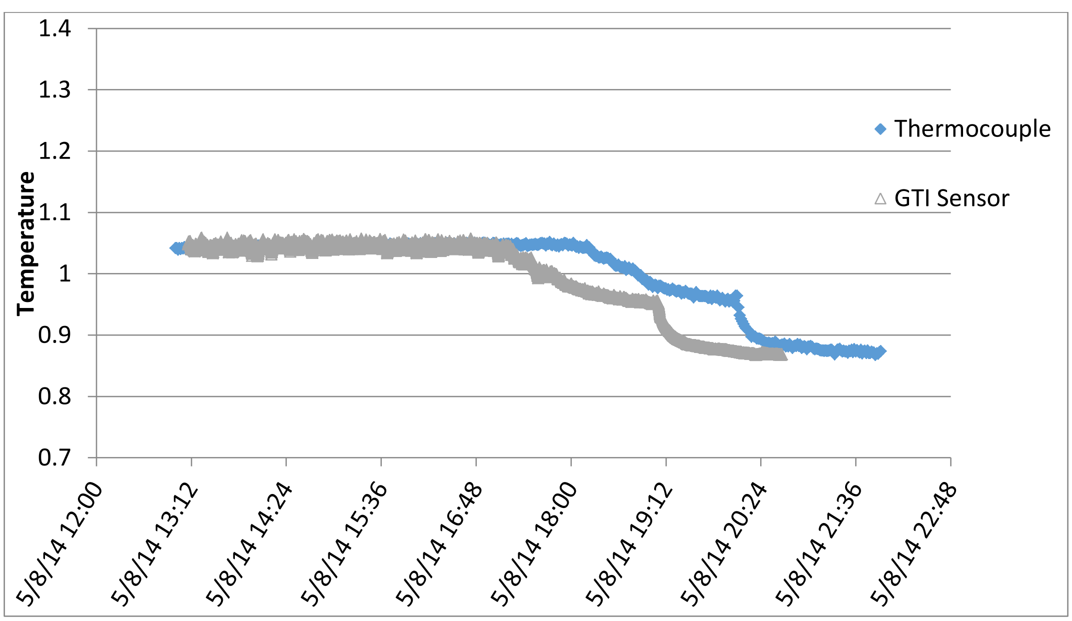

Figure 40. Comparison of temperature reading obtained with the gasifier

Figure 40 demonstrates a very good agreement between the temperature readings obtained with the thermocouple and the Gasifier Sensor. Apparently the Gasifier Sensor showed better response time detecting the temperature decrease sooner than the thermocouple. The temperature data obtained during the Gasifier Sensor testing and included in this report is presented in the non-dimensional form to protect the proprietary information related to the gasifier operation.

The GTI project team was not able to compare the temperature data obtained with the Gasifier Sensor with any other temperature measurements since no other means of direct measurement of the gasifier temperature were available. Figure 41 shows a comparison of the gasifier sensor temperature data and the temperature estimate calculated by the Wabash operators based on the gasifier downstream parameters (the "Wabash estimate"). As it can be observed from the figure, the gasifier sensor temperature readings are overall lower than the Wabash estimate. Also, the GTI sensor temperature data shows higher variability, which is most likely a reflection of a non-uniform temperature distribution of the highly turbulent flow of the gasified coal particulates.

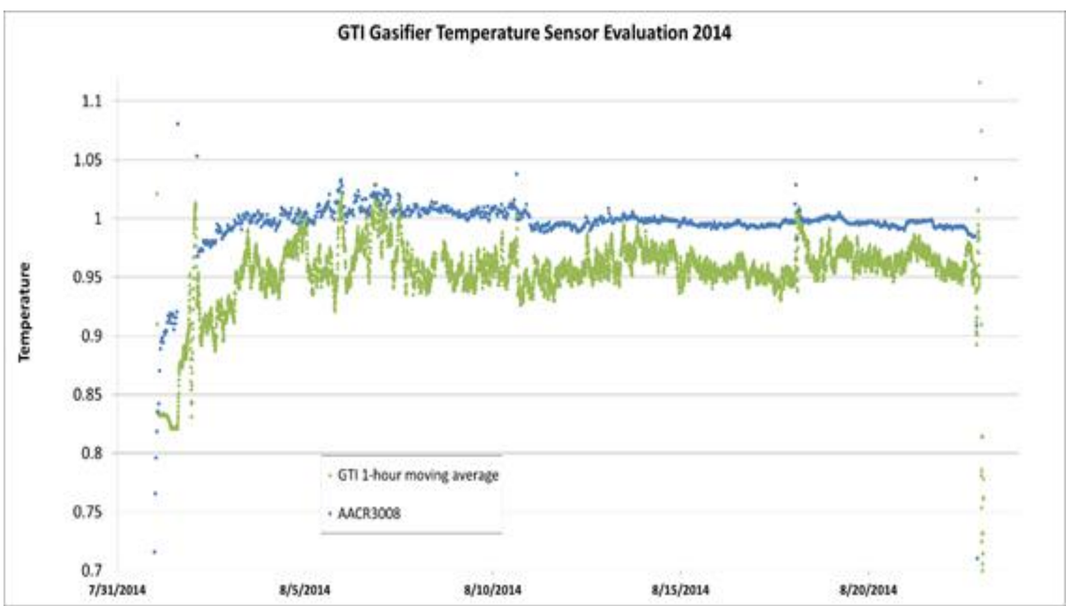

Figure 41. Comparison of Gasifier sensor readings with Wabash temperature estimates

Task 7.0 Development of Commercialization Plan

Y P Buch, Senior Vice President of Reliance Industry Refinery division contacted the project team and expressed interest in the developed sensor technology. Mr. Buch introduced GTI to LumaSense Technologies, developer and manufacturer of a variety of optical sensors for the global market. GTI and LumaSense are currently exploring the feasibility of the commercialization of the knowhow developed under the current and the prior projects.

The value of any sensor is centered on that sensor's ability to provide information that allows easier, safer, or more reliable operation of the process of interest. Sensors range from simple, low cost devices to complex devices serving limited but critical market applications. For a sensor to be commercially successful, the device must meet a market need but also must have broad enough market demand to justify development and sales costs.

The sensor demonstrated in this project provides a way to make non-contact readings of high temperatures in harsh environments. This information is crucial to optimized operation of a number of industrial processes. Variations of the sensor are expected to meet market demands in many of these markets. Some of these markets include:

- Coal and biomass gasification units
- Coal and biomass combustion boilers
- Incinerators
- Cement kilns
- Mineral wool cupolas
- Heat treating furnaces
- Glass furnaces
- Steel industry electric arc furnaces
- Steel reheat furnaces
- Chemical process heaters
- Power turbines
- Large-scale stationary engines

GTI intends to work with LumaSense to develop commercial prototypes of the sensor. Sensor beta prototype variations will be tested in multiple applications to demonstrate the power and flexibility of the sensor. Once reliability and cost benefits have been established, commercial versions of the sensor will be developed, sold, and supported. The team intends to apply the sensor as broadly as possible by identifying and exploiting promising market opportunities. Once proved and operating commercially, the team will expand marketing and sales into proven markets and then into new markets. An outline of the commercialization path includes the following steps:

1. Ranking of potential markets by order of intended first adoption
2. Development of beta prototypes of the sensor for target markets
3. Demonstration of beta prototypes of the sensor in target markets
4. Initial sale of commercial versions of the sensor in target markets
5. Repeat of commercialization path for other targeted markets

CONCLUSIONS AND RECOMMENDATIONS

All project objectives were accomplished on time and according to the project schedule.

The software specifications and temperature recognition algorithms have been developed. The final version of the sensor software has been implemented in the form of LabView code. The software was tested and debugged during the experimental runs at GTI by the GTI/NCSU team. The sensor was calibrated and prepared for the gasifier runs.

Numerical studies of the flow inside the optical channel of the gasifier probe were performed for the original design. The design modifications were suggested and tested numerically. The numerical results were further confirmed by the experimental tests.

Modification to the optical channel was proposed. The modified design had a purging obstruction in the optical channel in front of the optical window. The modified design did not alter the optical field-of-view of the sensor. The probe modification was implemented and tested at Wabash River gasifier. Even though the tested time period was shorter than the planned six months, the Gasifier sensor confirmed unobscured operation for the entire time interval of testing, which exceeded three months.

For proprietary reasons we have to limit the amount of pictures and data that can be published. Despite this limitation, the permitted data confirmed that the sensor has proved highly successful during long-term operation in a harsh environment with high temperature, high pressure, and high particulate loading. Major project conclusions include:

- Laboratory testing has found the new sensor to be as accurate and repeatable as contact temperature sensors

- The sensor can be controlled and the data can be collected and processed by an integrated software package
- The sensor works reliably for months installed in harsh environments of high temperature, high pressure, and high particulate content
- After conclusive proof in this project, the sensor is ready for development of final prototypes and first commercial units.

The project team will work with new partners to execute the commercialization plan and to deploy the sensor in places where no available sensors can survive.